#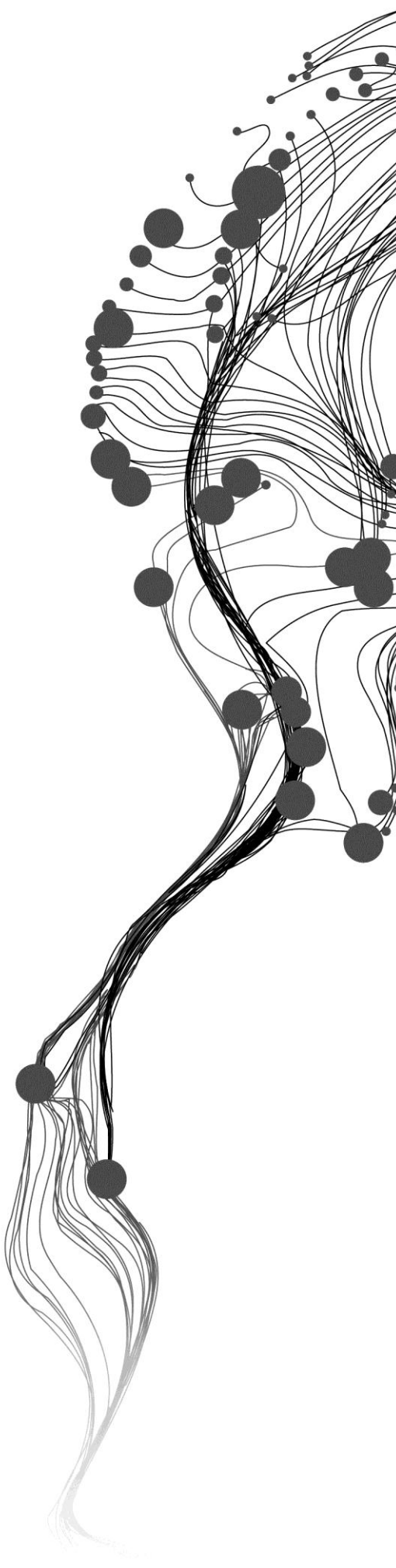 APPLICABILITY OF WAVELENGTH MAPPING METHOD FOR THE INTERPRETATION OF HYPERSPECTRAL IMAGES THE NILI FOSSAE REGION OF MARS

ZULFA ABDURAHMAN OMER
March, 2013

SUPERVISORS:
MSc. W.H. (Wim) Bakker
Dr. F.J.A.(Frank) van Ruitenbeek

APPLICABILITY OFWAVELENGTH MAPPING METHOD FOR THE INTERPRETATION OF HYPERSPECTRAL IMAGES OF THE NILI FOSSAE REGION OF MARS

ZULFA ABDURAHMAN OMER
Enschede, The Netherlands, March, 2013

Thesis submitted to the Faculty of Geo-Information Science and Earth Observation of the University of Twente in partial fulfillment of the requirements for the degree of Master of Science in Geo-information Science and Earth Observation.
Specialization: Applied Earth Science

SUPERVISORS:
MSc. W.H. (Wim) Bakker
Dr. F.J.A. (Frank) van Ruitenbeek

THESIS ASSESSMENT BOARD:
Prof. Dr. F.D. (Freek) van der Meer (Chair)
Prof. Dr. S.M. (Steven) de Jong (External Examiner, Utrect University)

ABSTRACT

Mars is an Earth-like planet having various mineralogical compositions associated with different rocks which are the results of different processes occurring on Mars. Understanding the surface mineralogy of Mars is the key to explore the history of Mars. However since there is no mechanism of ground-truthing of mineral mapping of Mars, spectroscopic remote sensing is the only way for exploring and understanding Mars.

Observatoire pour la Mine'ralogie, l'Eau, les Glaces et l'Activite´ (OMEGA) images of Mars which have been collected by the OMEGA hyperspectral sensor have been processed and interpreted to identify surface minerals of Mars. These images have a low resolution and may contain noise from various sources.

This research aims at investigate the applicability of the wavelength mapping method for interpreting OMEGA imagery for surface mineral identification of the Nili Fossae region of Mars. To achieve this objective the image has been preprocessed. The wavelength mapping method has been applied in order to take the advantage of the spectral as well as the spatial information content of the image and make the interpretation easier by making wavelength regions which represent different minerals. Subsequently the resulting wavelength regions which show some spatial patter have been used to interpret the image by creating regions which give enough information rather than concentrating on single pixel information and also to get better spectra having deep absorption features. These regions are used to aggregate the pixels and obtain mean spectra which can be compared with library spectra of USGS. On the other hand the wavelength map has been used in combination with MOLA data to observe the stratigraphic relationship between the minerals of the area. Finally the OMEGA image has been compared with CRISM images for validation purpose.

The result of the visual spectral comparison of the OMEGA image with library spectra of USGS showed similarity with candidate minerals: saponite, sepiolite, kaolinite and montmorillonite. In addition the comparison of OMEGA image with MOLA data (3D view map and geomorphologic map) shows the stratigraphic sequence of the minerals which have been identified from the spectral matching of OMEGA image and library spectra. The comparison of the spectra of OMEGA image with the spectra of CRISM images shows good correlation in the wavelength regions between 2.30-2.35 µm and also 2.20-2.25 µm. In general the wavelength mapping method has been illustrated to be applicable for the interpretation of OMEGA image in the Nili Fossae region of Mars.

Key words: Mars, OMEGA, CRISM, Wavelength Mapping, MOLA, geomorphology

.

ACKNOWLEDGEMENTS

TABLE OF CONTENTS

LIST OF FIGURES

LIST OF TABLES

LIST OF ABBREVIATIONS

CAT   CRISM Analysis Toolkit
CRISM   Compact Reconnaissance Imaging Spectrometer for Mars
DEM   Digital Elevation Model
MOLA   Mars Orbiter Laser Altimeter
OMEGA   Observatoire pour la Mine´ralogie, l'Eau, les Glaces et l'Activite´
PSA   Planetary Science Archive
ROI   Region of Interest
SWIR   Short Wavelength Infrared
VNIR   Visible and Near Infrared
USGS   United States Geological Survey
μm   micrometer

1. INTRODUCTION

1.1.   Background

Mars is an Earth-like planet of the solar system located near to the Earth. Due to that a lot of attention has been given to investigate for the origin and processes which are related to the evolution and make up of Mars. Many parts of the planet have been studied not only for research purpose but also to gather information about the planet and also to find landing sites for the rovers for acquiring information about the planet.

Exploring the mineral composition of Mars is an important issue for understanding the history of the planet (Murchie et al., 2000). In addition, this knowledge is crucial to understand the climatic and geologic history of the planet.
However to study the mineralogy of Mars in a broader sense the man-made satellites are the only sources of information. There are three satellites which are orbiting Mars at this moment are Mars Global Surveyor (MGS), Mars Odyssey, and the European Space Agency's Mars Express. These instruments are targeted and prepared to identify minerals on the Martian surface. In addition their main mission is to gather and send data to the Earth for analysis and research. And some of the components of the data that are being sent to the Earth comprise hyperspectral images of Mars having different resolutions and topographic information of Mars.

Spectroscopic remote sensing is an important means of differentiating lithologic units and in preparation of mineral maps. Different materials absorb the energy of light at their specific wavelengths due to electron, vibrational, or rotational processes and this makes it possible to identify different materials using their composition from hyperspectral imaging (Fan et al., 2012).

The SWIR (Short Wavelength IR) wavelength region of the Electromagnetic spectrum between 2.000 and 2.500 μm is appropriate for mineral mapping. For instance it shows many absorption features of certain hydroxyl- and carbonate-bearing minerals and hydrothermal alteration minerals (Thomas, 2002).

Hyperspectral images of the surface of Mars have been acquired from OMEGA (The Observatoire pour la Minéralogie, l'Eau, les Glaces et l'Activité), the European Space Agency/Mars Express visible/near-infrared (VIS/NIR) spectral imager, since it started its operation in January 2004 (Combe et al., 2008). The OMEGA hyperspectral images of the surface of Mars represent a great progress in Martian exploration, by providing spectral images for the first time on a global scale (Combe et al., 2008).

The OMEGA spectrometer consists of a VNIR(Visible and Near Infra Red) and two SWIR (Short Wavelength IR) spectrometers and the different observations must overlap to create one continuous spectrum (Mangold et al., 2007a). OMEGA provides hyperspectral images of the surface of Mars with a spatial resolution ranging between 0.3 and 4km/pixel in 352 contiguous spectral channels in the visible and near-infrared range, between 0.3 and 5.2 μm (Bibring et al., 2004).

The main task of the instrument was to map several important minerals which have great contribution to investigate Mars (Bibring et al., 2005a; Bibring et al., 2006). The OMEGA data helped to produce a global map which shows a more complete view of the Martian materials (Poulet et al., 2007). Several OMEGA orbits of low and high spatial resolutions cover the whole Nili Fossae–Syrtis Major regions (Mangold et al., 2007a) which is important for this thesis.

1.1.1.   CRISM images

The Compact Reconnaissance Imaging Spectrometer for Mars (CRISM) (Mustard et al., 2007) is a visible and near infrared hyperspectral imager on the Mars Reconnaissance Orbiter (MRO) and has been operating on Mars since 2006 (Murchie et al., 2009). CRISM has a spectral range from 362 to 3920 nm with 6.5 nm spectral sampling. The instrument has two primary observing modes: hyperspectral observations, which are acquired in 544 channels at a high spatial resolution (around 20 to 40 m/pixel) and survey multispectral observations, which are acquired in 72 channels at a reduced spatial resolution (around 100 to 200 m/pixel) (Murchie et al., 2007).

1.1.2. MOLA data

The Mars Orbiter Laser Altimeter (MOLA) (Smith et al., 1998; Zuber et al., 1992) is an instrument on the Mars Global Surveyor(MGS) spacecraft. Mola started its operation on Mars surface on September 1997 and it can capture the surface features at a maximum vertical resolution of 30cm and an along-track spacial resolution of 300-400m (Smith et al., 1998). The main purpose of MOLA data is to characterize surface topography, roughness, and 1.064 mm wavelength albedo of Mars surface. It mapped the topography of Mars (Neumann et al., 2003).

1.2. Research Problem

Satellites from ESA and NASA have been collecting hyperspectral imagery of the surface of Mars since 1962(refer?). Interpretation of these images provides mineralogical information of its surface. Different approaches have been applied on OMEGA image to interpret the surface minerals of Mars. However, although a number of publications about the surface mineralogy have appeared in the international literature the interpretation of the imagery is still challenging. Furthermore the mineral maps obtained from the image are open for re-interpretations due to many factors related to the image itself and the methods which are applied on the image.

And one of the reasons could be that OMEGA has spectrally mapped Mars at lower spatial resolution and it has instrument specific problems and also interference of Martian atmosphere (Bakker et al., 2009;Bibring et al., 2005a; Daswani, 2011). Hence due to the nature of the OMEGA image with regard to noise, resolution and presence of instrument artifacts, the images might not give reliable results in application of common and/or standard image analysis techniques. The lack of such accuracy and inconsistency shows that the quality of the image and the applied analytical method are not compatible. For instance the spectral angle mapper (SAM) method showed low correlation between the extracted spectra and the laboratory spectra when it is applied on OMEGA images (Daswani, 2011).

Both the low resolution of OMEGA image and the noisy character of the data make it challenging to do minerals interpretation of on Mars.

1.3. Research Problem

1.3.1. General objective

The main objective of this research is to prove the applicability of the wavelength mapping method for surface mineral interpretation of OMEGA image of Nili Fossae region of Mars.

1.3.2. Specific objectives

➢ To extract spectra from OMEGA imagery and to compare with library spectra of USGS.

> To investigate the stratigraphy of the minerals identified by draping the wavelength map on 3D view map of MOLA data.
> To compare the spectra of OMEGA image with the spectra of CRISM images.

> To validate the results obtained from interpretation of OMEGA image with the results that can be found in other literatures.

1.4.　　Research questions

- What information can be extracted by comparing the spectra retrieved from OMEGA image with spectral libraries of USGS?

- What can we extract by comparing the wavelength map from OMEGA image by draping 3D draped on MOLA data and geomorphologic map?

- What can we conclude by comparing the spectra extracted from OMEGA imagery with that of CRISM images?

- What can we conclude by comparing the results of the research with the results of other researches?

- Is wavelength mapping method applicable for mineralogical interpretation of OMEGA imagery in Nili Fossae region of Mars?

1.5.　　Research hypothesis

It is possible to use wavelength mapping method and other techniques to interpret OMEGA imagery for mineral identification by applying different techniques.

1.6.　　Outline of the thesis

The thesis consists of seven chapters, chapter one is the introduction containing the background, research problem, research hypothesis, research general and specific objectives, research questions and outline of the thesis .Chapter two provides a literature review on mineralogy, geology and geomorphology of the study area as a review. Chapter three describes the study area, materials, methods and conceptual framework of the work. Chapter four describes the preprocessing steps of the images used in the research. Chapter five focuses on the data analysis and results obtained to answer the research objectives. Chapter six focuses on discussion of each result. Chapter seven gives conclusions and recommendation of the research.

2. LITERATURE REVIEW

This chapter deals with literature review on the geology, geomorphology and mineralogical settings of the study area as well as on remote sensing for mineralogical mapping.

2.1.   Location of the study area

Nili Fossae is a tectonic graben striking in the NE-SW direction (Wichman and Schultz, 1989) related to the Isidis impact basin in the Northeastern hemisphere of Mars (Mangold et al., 2007). The region is located at 17° to 27°N latitude and 70° to 80°E longitude (Figure 2-1). The Nili Fossae region of Mars is selected for this thesis because this part of Mars is interesting for geological investigations (Schaber, 1982) and because abundant phyllosilicates are mapped by the OMEGA spectrometer in this region (Bibring, 2005; Poulet et al., 2005).
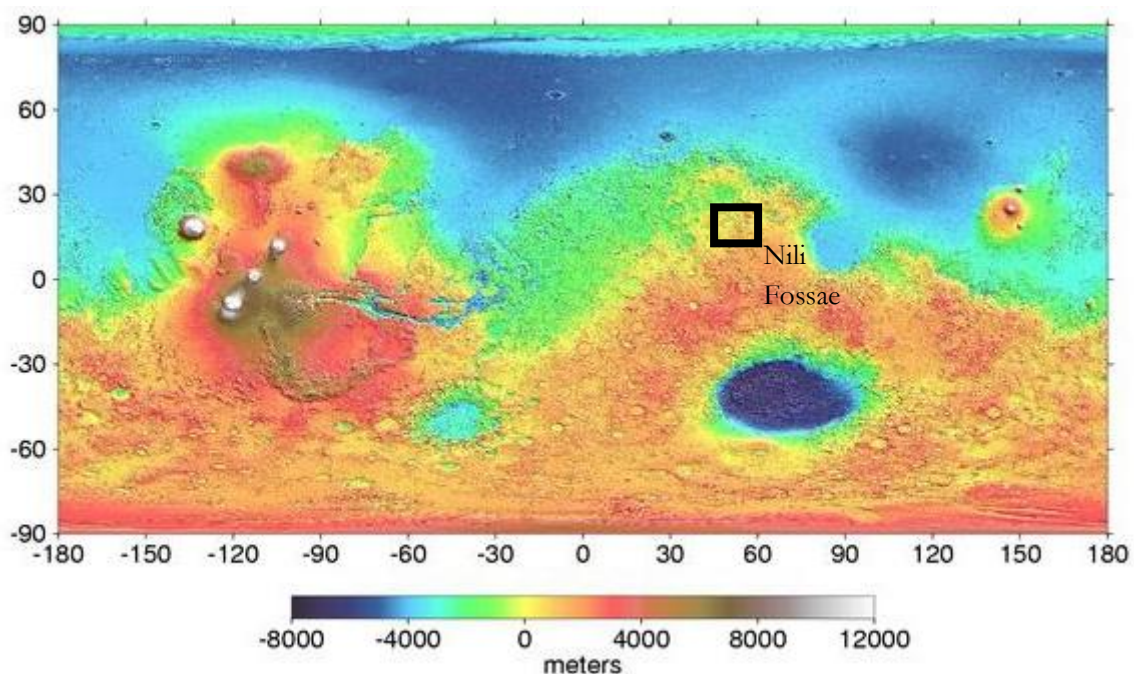
Figure 2-1: Location map of the study area on Global topographic map of Mars based on MOLA data and the black box marks the location of the Nili Fossae area

2.2.   Geology and mineralogic setting of Nili Fossae area

The Nili Fossae region exhibits a complex geology that provides insight into the processes operated during the early history of Mars. The excellent exposure of bedrock outcrops through portions of this region permit direct association of mineralogy and lithology, and morphology (Mustard et al., 2007). The regional geology is composed of two main units: ancient (Noachian) basaltic crust which is modified by impact and dissected tectonically and, younger (Hesperian) Syrtis Major basaltic lava plains (Mangold et al., 2007) and the contact between these lithologic units is marked by a distinct compositional boundary (Ehlmann, 2009).

From OMEGA spectra it has been evidenced that the Syrtis Major lavas are basaltic in composition and rich in high-calcium pyroxene (Bandfield, 2002; Mustard et al., 2007; Poulet et al., 2009), while the Noachian cratered terrains are basaltic in composition dominated by low-calcium pyroxene-bearing materials (Mustard et al., 2007; Poulet et al., 2009).

The eastern part of Nili Fossae shows high exposure of olivine-rich rocks (Hamilton and Christensen, 2005; Hoefen et al., 2003; Poulet et al., 2007) and these rocks are partially altered in some places to Mg-carbonate (Ehlmann et al., 2008a). In addition the presence of carbonates and clays could be an indication of the presence of neutral to alkaline water at the time of their formation and that the acidic weathering which is suggested to the part of Hesperian age process, did not affect them and did not dominate all aqueous environments(Ehlmann et al., 2008b).

However in some places the olivine-rich unit shows absorption features at 1.91 and 2.32 μm, due to H2O and Mg-OH respectively with a weak feature at 2.5 μm (Mangold et al., 2007b; Mustard et al., 2007) and this combination of absorptions represents Mg-rich phyllosilicate, either saponite or serpentine rather than carbonate (Ehlmann et al., 2010). In addition Ehlmann et al. (2009) mentioned the Mg-carbonate and kaolinite bearing rocks overlying the Fe/Mg smectite-bearing units.

Below the carbonate-bearing unit lies a regionally extensive, Fe-Mg smectite-bearing stratigraphic unit (Mangold et al., 2007a; Mustard et al., 2007) and this unit is associated with talc in the eastern part of Nili Fossae area (Mangold et al., 2007b). Mangold et al. (2007) discussed a stratigraphically lower Mg-phyllosilicates bearing unit in many locations throughout Nili Fossae and it has been associated with the mineral saponite with spectral match to the 2.315 and weak 2.39 μm band.

Although many different types of phyllosilicates minerals have been identified by surface mineral mapping using short wave infrared spectroscopy CRISM and OMEGA, large abundances of sulfate minerals are not detected in the Nili Fossae region (Ehlmann et al., 2008a; Ehlmann et al., 2010).

3.   MATERIALS AND METHODS

This chapter discusses the methods that have been used in order to analyze the data in accordance to the goal of the study.

3.1.   Materials

The overview of the data sets that has been used in this research include Observatoire pour la Mineralogie, l'Eau, les Glaces et l'Activite´ (OMEGA), Compact Reconnaissance Imaging Spectrometer for Mars (CRISM), and Mars Orbiter Laser Altimeter (MOLA) and spectral libraries of USGS.

Table 1: Table showing the software used in this research

Software	Purpose
PSA Browser	dataset searcher on the Planetary Science Archive (PSA)
SOFT07	the OMEGA science team's software in IDL for calibrating OMEGA images and it was obtained from PSA
ALPHA	a graphical user interface (GUI) for SOFT05 by van der Werff
IDL Workbench 7.8	to use SOFT05 and Alpha
HypPY	for the purpose of viewing and preprocessing images, which also implements a number of preprocessing corrections designed for OMEGA and CRISM images from python program by Bakker.
ENVI 4.8	for processing and visualizing images
CAT 7.2	for preprocessing of CRISM images
ArcGIS	for processing the MOLA data and the images and for preparing output maps
ILWIS 3.2	for producing stereo images from MOLA and OMEGA images
Google Earth	To visualize images with topographic features

The following shows the conceptual framework of the methods of the thesis
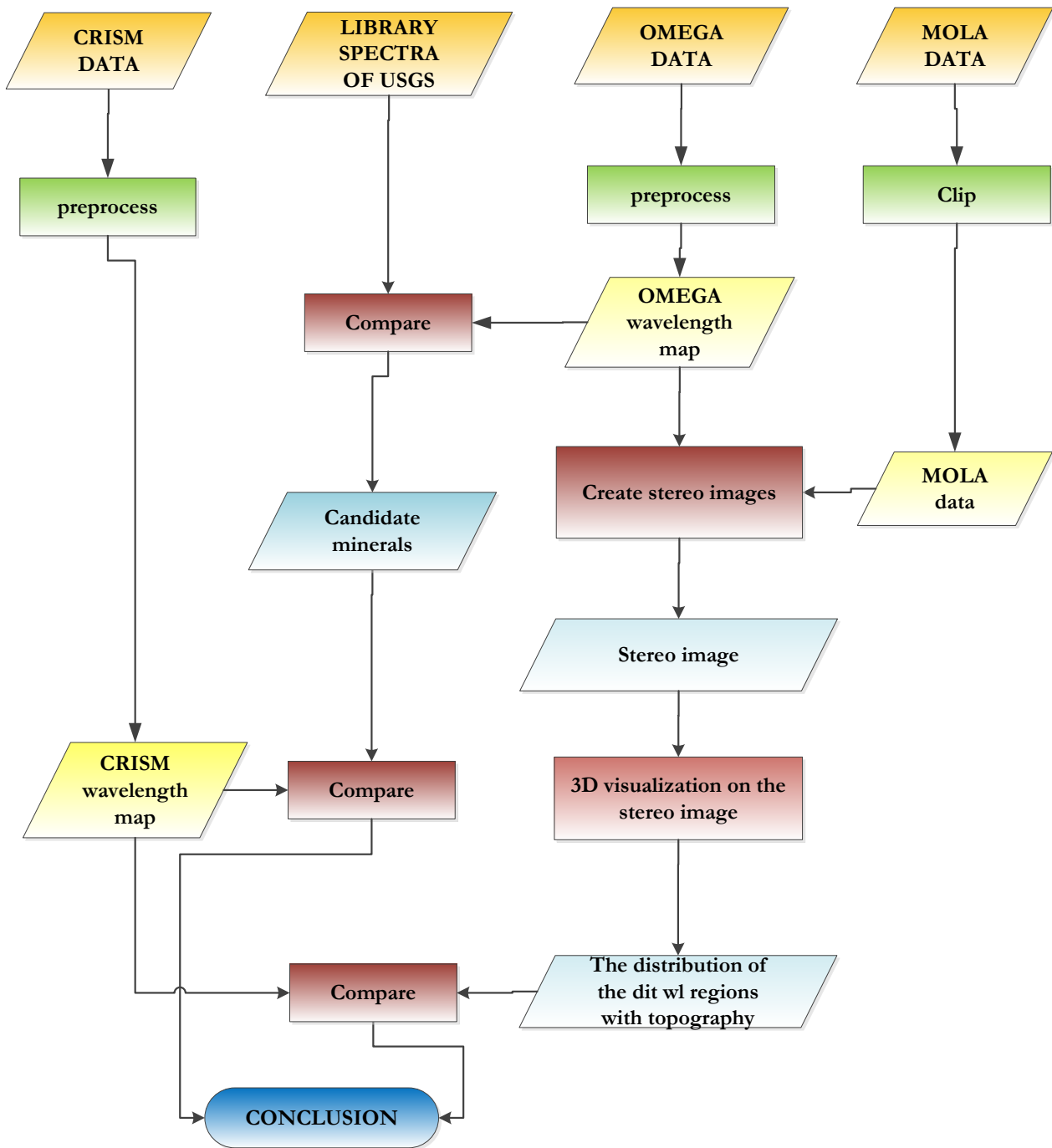
Figure 3-1: The work flow of the method of this thesis

3.2. The processing of OMEGA(ORB0232-2) data

Raw data and calibration

A single OMEGA (ORB0232-2) scene of Nili Fossae area has been downloaded from ESA's Planetary Science Archive (ESA PSA) in combination with the SOFT07 file in Alpha Interactive Data Language (IDL) routines. In order to make the data convenient and easier for interpretation different preprocessing techniques have been applied on the data. The preprocessing procedures are similar to the processing of hyperspectral images of Earth. The only difference being that these processes are targeted for Martian images specifically OMEGA images. The processing scheme is devised by Bakker et al., 2011 and the preprocessing chain is shown in Figure 3-2.

In order to convert the digital numbers in the original files into irradiance data which is radiometric calibration of the data has been done in Alpha Interactive Data Language (IDL) routines. This step helps to remove various instrument artifacts. This data obtained are jdat file (calibrated at sensor radiance) and geocube file (geometric data) together with other files. The rest of the preprocessing has been done on HypPY software.

The calibrated at sensor radiance file (jdat file) which is the main source file for geometric correction, solar correction and band masking processes. The Band masking which uses a signal to local business ratio (SLBR) for detecting noisy bands has been applied on the calibrated at sensor radiance file based on a certain threshold value in after exploring the noisy bands. The masking process helped to remove the bad bands from further analysis and correction The output of this process are good and bad bands and the bad bands are recorded in the bad bands list (BBL) of the image and only the header information is changed and nothing is changed on the images data itself.

After masking the bad bands the next step done was geometric correction of the calibrated at sensor radiance file using the geocube file which contains the geographic information of OMEGA image. Thus after geometric correction, the image to subset the image to the wavelength range of 2.0 to 2.5 micrometers. Then solar correction has been done on the subset data followed by atmospheric correction. Finally the absolute reflectance image has been obtained.

The second preprocessing procedures was log residuals which is a two-step normalization method in which the spectra of the pixels were normalized first and then pixels are divided by the mean spectrum of the whole image to get the pseudo reflectance image. The pseudo reflectance data was processed for spectral filtering using the fast mean 1-5-1 method. The minimum wavelength calculation was done to get the wavelength of minimum image which contains depth and wavelength values of the different absorption features of the image. Then the wavelength mapping method has been applied on the wavelength of minimum image to get wavelength map.
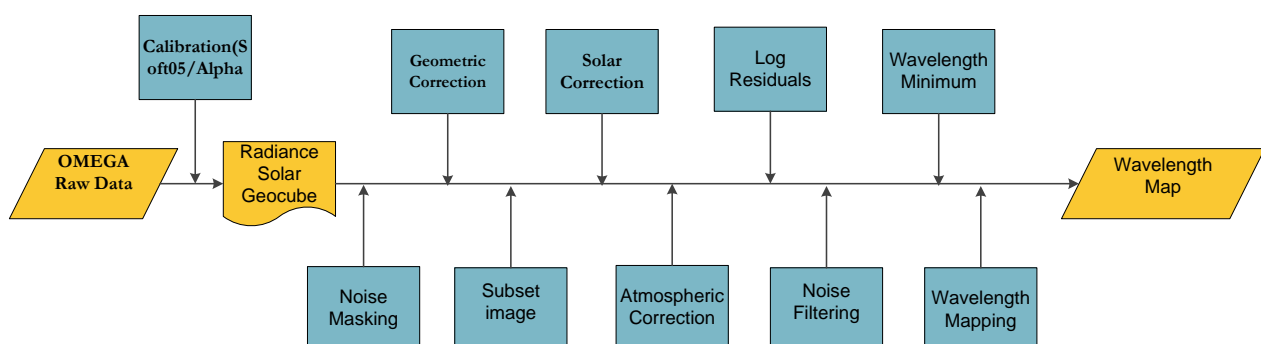
Figure 3-2: Summarized preprocessing scheme of OMEGA imagery, adapted from the processing chain by Bakker et al., 2011

In the next sections the wavelength of minimum and the wavelength mapping procedures will be discussed in more detail.

3.3. Wavelength of Minimum

Wavelength of Minimum is an algorithm by which the wavelength position of the deepest absorption feature of a spectrum is identified automatically. The algorithm searches for location in the spectrum where the most dominant absorption feature is found and then extracts its depth and width (Oluwadebi, 2011). In this research, the SWIR region of the Electromagnetic spectrum which has been analyzed in the wavelength ranges from 2.0 to 2.4 µm. The technique generates an output image of several bands, each band having information useful for identifying alteration minerals (Bakker et al., 2009) and other minerals. For this thesis the output bands which are important inputs for processing Wavelength Mapping are: interpolated minimum wavelength (i.e. wavelength of the minimum of the interpolated parabola) and interpolated depth (i.e. depth of the parabola at the minimum). The interpolation method uses information from three adjacent bands rather than just one central band.

3.4. Wavelength of Minimum

Wavelength Mapping is an algorithm which makes use of the output from wavelength of minimum to produce a color map and this is done by making use of color table and hue saturation values (HSV) of the interpolated wavelength of minimum and the interpolated depth of the feature (Oluwadebi, 2011). The wavelength range used for this process ranges between 2.1 and 2.5 µm. This algorithm is very useful in mineral interpretation and usually generates a mineral map with different colors which represents different wavelength absorption features and it is mostly useful in areas with alteration zones (Bakker et al., 2009).

In the next section the processes and data analysis which have been done on wavelength map and wavelength of minimum to extract spectral features will be discussed in more detail.

3.5. 2D scatter plot, Band Math(Boolean Logic) and creating ROI

The data analysis has been done on ENVI software.

The wavelength map which contains different wavelength regions has to be further processed and analyzed before interpreting the whole image. As it is clear from the image there are wavelength regions which represent absorption depth features of different minerals. Thus first of all the threshold depth of these absorption features of the different wavelength regions has to be known. Those features with shallow absorption depth are more prone to be covered by noise from different sources. Again those regions which are found at the edges of the wavelength range will be discarded because they are related to instrument artifacts when it measurement start and stops. But those regions which have at least depth range above 2% will be considered in the further steps of the data analysis.

Thus the wavelength regions with depth of absorption above 2% (three regions) were considered for extracting by combining the threshold depth obtained and the wavelength ranges to obtain the location of the regions. Then the resulting image will be used to create regions which represent that location the wavelength region having depth of absorption strong and discriminates those areas which have shallow depth and helps to reduce the noise which could come mixed with shallow depth spectral features.

Now the region which shows location of strong spectral features will be selected to create ROI to reduce the noise and get average spectra of that wavelength region. After that it is possible to compare with other source to

see and interpret the image based on spectra features of that specific region. WE can see that this step tried to reduce the noise but still there is a possibility of noise that's why we see random distribution of pixels on the two regions (2.20-2.25 µm) and are not following a certain pattern. Based on this the three regions have been passed through band math, creation of roi and computing the average spectra.

Now we can interpret the wavelength regions based on their spectra by comparing with reference spectra. The 2D scatter plot has been done using the interpolated wavelength of minimum (x-axis) and the interpolated depth (y-axis) images to get the threshold values for the depth of absorption features of the different wavelength regions of the wavelength map.

After the depth threshold has been obtained from the 2D scatter plot, the Band Math (Boolean Logic) has been applied on each wavelength range based on the threshold depth values in order to extract the location of the deepest absorption features of each wavelength range of the wavelength map. Again the pixels of the result of the Boolean Logic were aggregated (create ROI) in order to reduce the noise from that wavelength region and also to extract better spectral features. And then the mean spectrum of each ROI has been computed to compare with the USGS library spectra to identify minerals.

The next section presents the comparison of the mean spectra of the three wavelength regions with library spectra.

3.6. Comparison of spectra of OMEGA image(ORB0232-2) with library spectra

Spectral libraries are the main sources which are used as references to compare and identify surface mineral composition from hyperspectral images. One of the spectral libraries and the most widely used spectral libraries for the remote sensing application are the USGS. The speclab06 from USGS of selected minerals has been used for this research.

The mean spectra of the ROIs of each wavelength region of the wavelength map from OMEGA image (ORB0232-2) has been computed using the absolute reflectance image. Then the mean spectrum of the ROI of each wavelength region (2.20-2.24, 2.25-2.30 and 2.30-2.35 µm) the OMEGA image has been compared with library spectra of USGS of different minerals. The most prominent absorption features of the mean spectra of the roi image and from the library spectra were compared to identify the minerals in the study area.
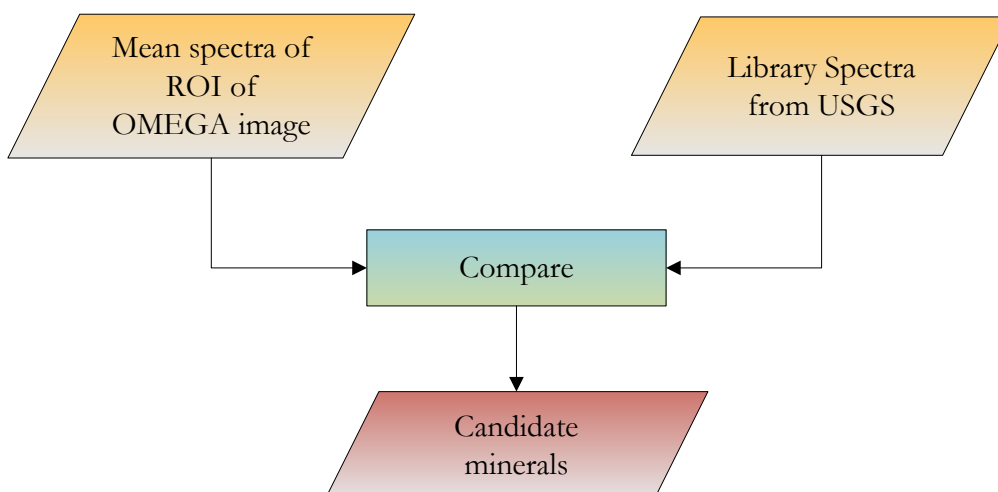
Figure 3-3: Flow chart showing the comparison of spectra of the reflectance image with library spectra

Since there are many minerals in the spectral library of the USGS, in order to simplify the comparison with OMEGA image spectra the library minerals were chosen based on the look up table which show the possible candidate minerals which can be interpreted from wavelength map of OMEGA image(ORB0232-2) (Figure 3-4). Some of the minerals selected for the wavelength region between 2.30-2.35µm are Fe-Mg clays (saponite, sepiolite, nontronite, hectorite, actinolite and antigorite), chlorites and serpentines. Some of the minerals selected for wavelength region between 2.25-2.30 µm are jarosite and nontronite. Some of the minerals selected for the wavelength region between 2.20-2.25 µm are Al clays (kaolinite, montmorillonite, muscovite, chalcedony, dickite and illite) and white micas.
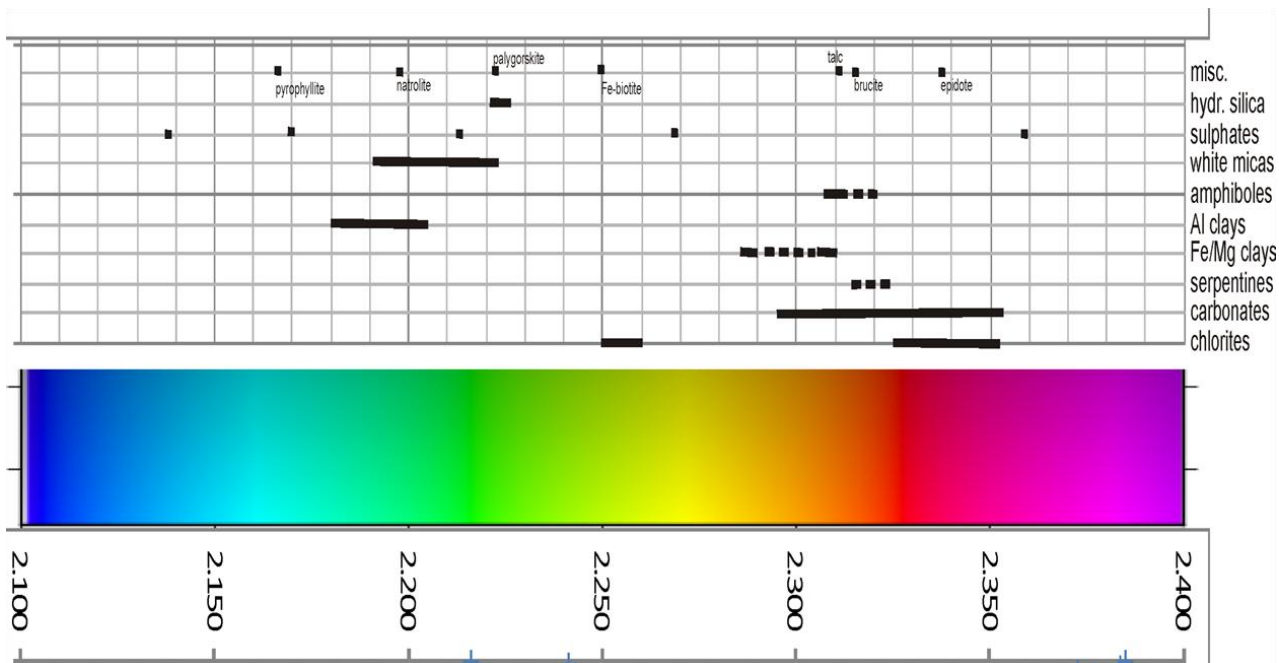
Figure 3-4: Look up table showing minerals from the USGS library with the legend of the wavelength map

3.7.   Comparing OMEGA image(ORB0232-2) with MOLA data

In this part of the method which is applied on the research, the wavelength map has been analyzed in combination with MOLA data has in order to explore the stratigraphic relation of the minerals identified from the visual spectral comparison of OMEGA image with library spectra.

The wavelength map from OMEGA image (ORB0232-2) and the Mars Orbiter Laser Altimeter (MOLA) data are defined with projection Mars_2000_sphere and re-projected to User Defined Equidistant Cylindrical projection. In order to create a stereo image from the wavelength map of OMEGA image (ORB0232-2) and the MOLA data, the MOLA data has been clipped and then it has been exported to with the wavelength map to ILWIS software both in tiff format and then the wavelength map has been linearly stretched and resampled to MOLA data to create the stereo image. The 3D visualization has been done to explore the relation of the different wavelength regions with different topographic and geomorphologic features.

In ArcGIS the MOLA data has been processed to generate shaded relief which helped to classify the area into different geomorphologic units in combination with contour map. The geomorphologic map produced contains

different units incorporating crater floors, graben floor, crater rims, walls of craters and graben, troughs and highland plains.
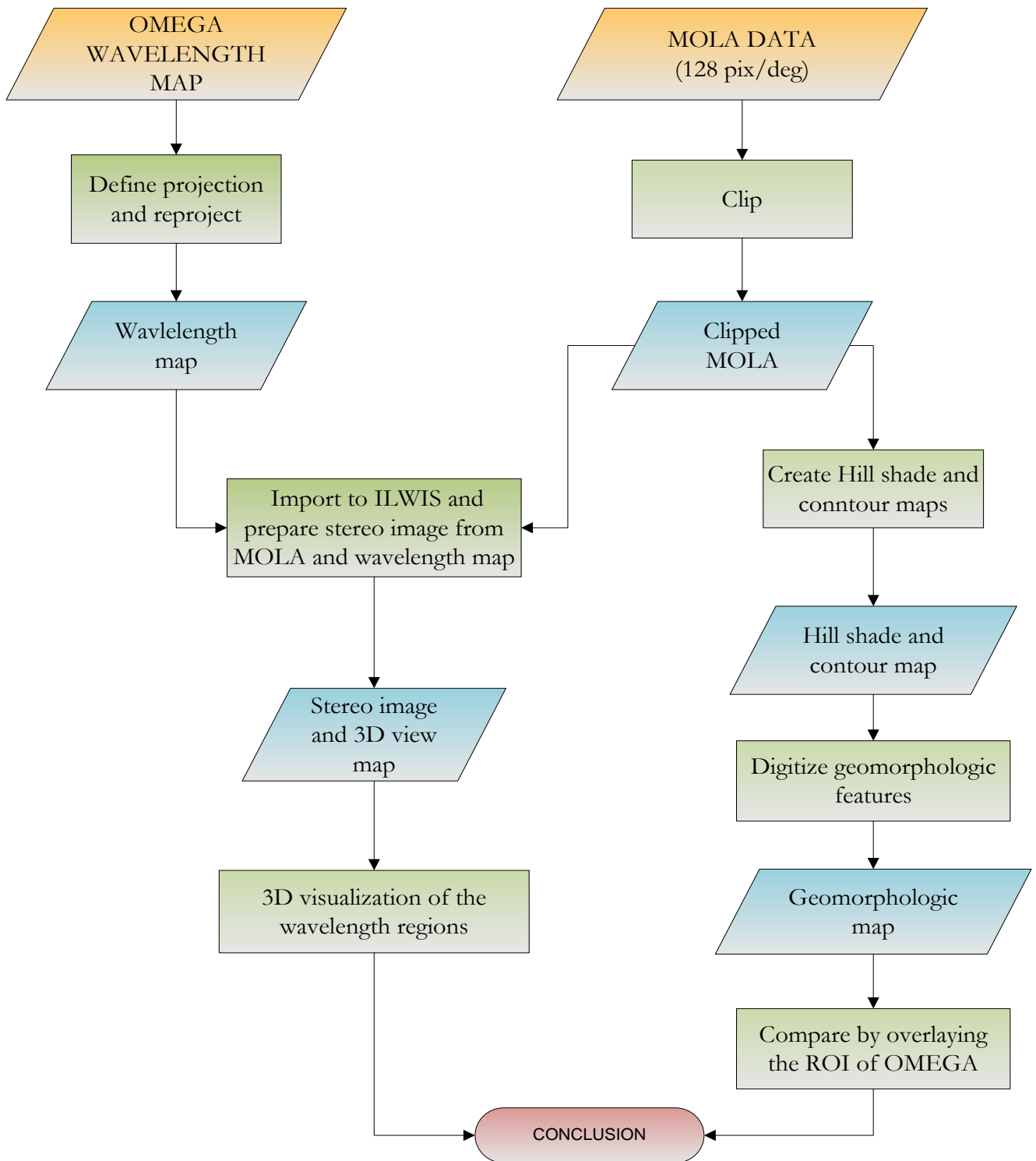
Figure 3-5: Flow chart showing the 3D visualization of the wavelength map

3.8.   Validation of OMEGA image (ORB0232-2) using CRISM image

Three CRISM data sets have been downloaded from NASA's CRISM Data Products (NASA CDP). In order to make the data convenient and easier for interpretation different preprocessing techniques have been applied on the data. The preprocessing of CRISM data is similar to that of OMEGA except that CRISM Analysis Toolkit (CAT) is available at the PDS Geosciences Node (http://geo.pds.nasa.gov/missions/mro/CAT_v6_7.zip) and it works imbedded in ENVI software.

Unlike the OMEGA data, the CRISM data is already calibrated to radiance or reflectance. The first part of the preprocessing after downloading the data is, converting the PDS data to CAT format. The CAT image has been atmospherically corrected on CAT software. The resulting image has been geometrically corrected and also masking of the bad bands has been performed. The corrected image has been reduced to wavelength range between 2.0-2.5 µm and fast mean 1+5+1 filtering has been done on it. The rest of the preprocessing steps, wavelength minimum and wavelength mapping have been done on HypPY software. And the results of these processes are wavelength of minimum and the wavelength map image. Figure 3-6 shows the preprocessing chain of CRISM images.
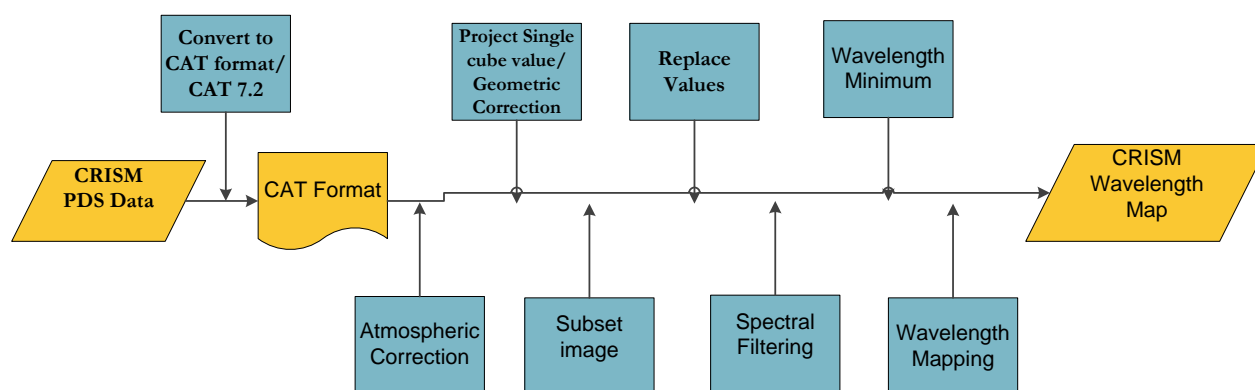
Figure 3-6: The preprocessing scheme of CRISM image, adapted from the processing chain by Bakker et al., 2011

In the next section the processes and data analysis which have been done on wavelength map and wavelength of minimum of each CRISM image to extract spectral features for the purpose of comparing with OMEGA image will be discussed in more detail. Figure 3-8 shows the comparison steps taken between the spectra of the ROI of OMEGA (ORB0232-2) and CRISM images.

3.8.1.   Validation of OMEGA image (ORB0232-2) using CRISM (FRT0000A053) images

The CRISM image (FRT0000a053) is found at the center of the crater and its ROIs have been compared with the ROI of OMEGA image (ORB0232-2) to validate the minerals identified in the crater. The procedure to create ROI have been also applied on this CRISM image (FRT0000a053) in order to compute mean spectra of ROI of CRISM image for comparing with the spectra of ROI of OMEGA image. And then the mean spectra of the ROI of this CRISM image (FRT0000A053) have been compared with the ROI of OMEGA image (ORB0232-2).

3.8.2.   Validation of OMEGA image (ORB0232-2) using CRISM (FRT00009971) images

This CRISM image (FRT00009971) is found at the edge of the crater and the graben and its ROIs have been compared with ROI of OMEGA image. The procedure to create ROI have been also applied on this CRISM image (FRT00009971) in order to compute mean spectra of ROI of CRISM image for comparing with the

spectra of ROI of OMEGA image. And then the mean spectra of the ROI of this CRISM image (FRT00009971) has been compared with the ROI of OMEGA image (ORB0232-2).

3.8.3. Validation of OMEGA image (ORB0232-2) using CRISM (FRT000064D9) images

This CRISM image (FRT000064D9) is located at the floor of the graben and its ROIs have been compared with ROIs of OMEGA image. The procedure to create ROI have been also applied on this CRISM image (FRT000064D9) in order to compute mean spectra of ROI of CRISM image for comparing with the spectra of ROI of OMEGA image. And then the mean spectra of the ROI of this CRISM image (FRT000064d9) have been compared with the ROI of OMEGA image (ORB0232-2).

4.   RESULTS

In this chapter the results obtained from the different processes of the OMEGA (ORB0232-2) and CRISM images using the methods described in chapter 3 will be discussed. In the first section of this chapter the results of the preprocessing of the data of OMEGA (ORB0232-2) image will be discussed. In the second section the results of the comparison between the spectra of OMEGA (ORB0232-2) image with library spectra will be discussed. In the third section the results of the comparison between the wavelength map with geomorphologic map and 3D view map will be discussed. In the fourth section the results of the comparison between OMEGA (ORB0232-2) and CRISM images will be discussed.

4.1.   Results of the preprocessing of OMEGA(ORB0232-2) data

There are many steps which have been taken to preprocess the OMEGA image (ORB0232-2) the data (section 3.3) before it has been compared with other datasets for mineral identification. OMEGA imagery is a low resolution image and contains noise from the instrument itself and other sources. Thus the preprocessing steps have been done to calibrate and correct the data, and also to reduce the noise from the image. Even though the image has passed through such steps there are still noisy pixels observed on the image. In addition this is related to the absorption depth of the features being shallow not to see the features clearly for interpretation of OMEGA image.

The wavelength mapping algorithm is an important tool that shows overview of distribution pattern of spectra of different materials in the area. The combination of the interpolated wavelength of minimum with the interpolated depth of the features in this algorithm pointed out which absorption features is dominating each pixel. The resulting map, wavelength map, (Figure 4-1(a)) shows image with different colors symbolizing various absorption feature wavelengths, each color representing degree of saturation at different absorption depth.

The degree of color saturation of the wavelength map is a factor of the depth of absorption. Due to this similar spectra which have the same wavelength position of absorption feature will show slight changes in color saturation as a result of different depth of absorption which means at higher depth, the color becomes brighter while at lower depths the color becomes darker. Figure 4-1(b) shows differences in color saturation in similar spectra as a result of different depths of absorption. As it is observed on the wavelength map, the pixels have spatial coherence at the center of the image while the pixels outside that area do not have spacial coherence which indicates that there is important information as well as noise mixed in the image.

Thus the wavelength mapping tool played great role to overcome and show some patterns of pixels which follow a certain structure to invite for further interpretation by looking at some patterns on the image which follow a certain structure. However it is difficult to extract information from a single pixel, so interpreting a bunch of pixels or a region will help and minimize the noise before interpreting the wavelength map. Thus creating Regions of Interest (ROI) helped to minimize the noise from the image and also to get mean spectra.

The 2D scatter plot (Figure4-1(c)) which has been done from the interpolated wavelength of minimum and the interpolated depth images shows the distribution of the different pixels over the wavelength map to show the relation of the range of absorption depth with wavelength range. Thus as it is shown on the plot the wavelength range between 2.25-2.31 has strong absorption depth (>4%) while the other wavelength regions (2.20-2.25 and

2.31-2.35) have shallow absorption depth (<4%) and also this wavelength range shows spacial coherent pattern unlike the other wavelength regions which show random distribution. The wavelength range below 2.20 µm and above 2.350 µm has been left out because the spectra of this wavelength range are rarely seen on the image and could be representing random noise and instrument artifacts. In addition the darker part of the image at the northern part of the study area has been left out because the area shows dark color and due to this it does not show clear spectra.
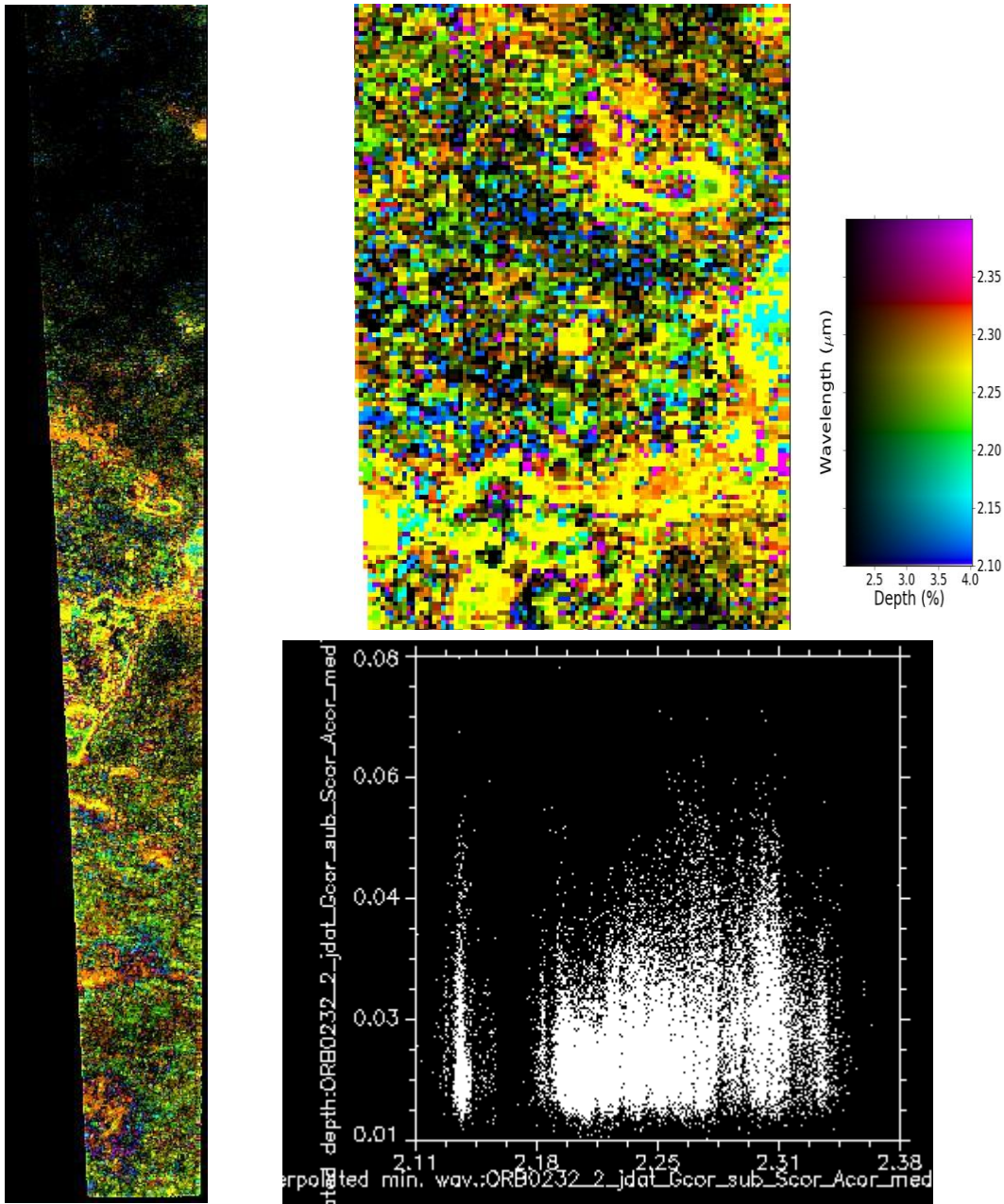
Figure 4-1: (a) Wavelength map of the OMEGA image (ORB0232-2) of the study area (b) Wavelength map showing the difference in color saturation with depth (c) 2D scatter plot from interpolated wavelength of minimum image(x-axis) and the interpolate depth(y-axis)

Thus the wavelength range has been classified in to three ranges based on depth. Each ROI has been obtained after the Boolean logic of each wavelength range has been computed according to the depth threshold of each wavelength range from the 2D scatter plot. Thus the ROI of the different wavelength regions have been created based on the result of the Boolean logic and three ROI has been created in the wavelength range 2.0-2.25, 2.25-2.30 and 2.30-2.35µm and their mean spectra has been computed according to the procedure explained in chapter 3 section 3.5 in order to compare their spectra with library spectra. Figure 4-2 presents all the ROI of the different wavelength regions draped over the absolute reflectance image (band 2.314).
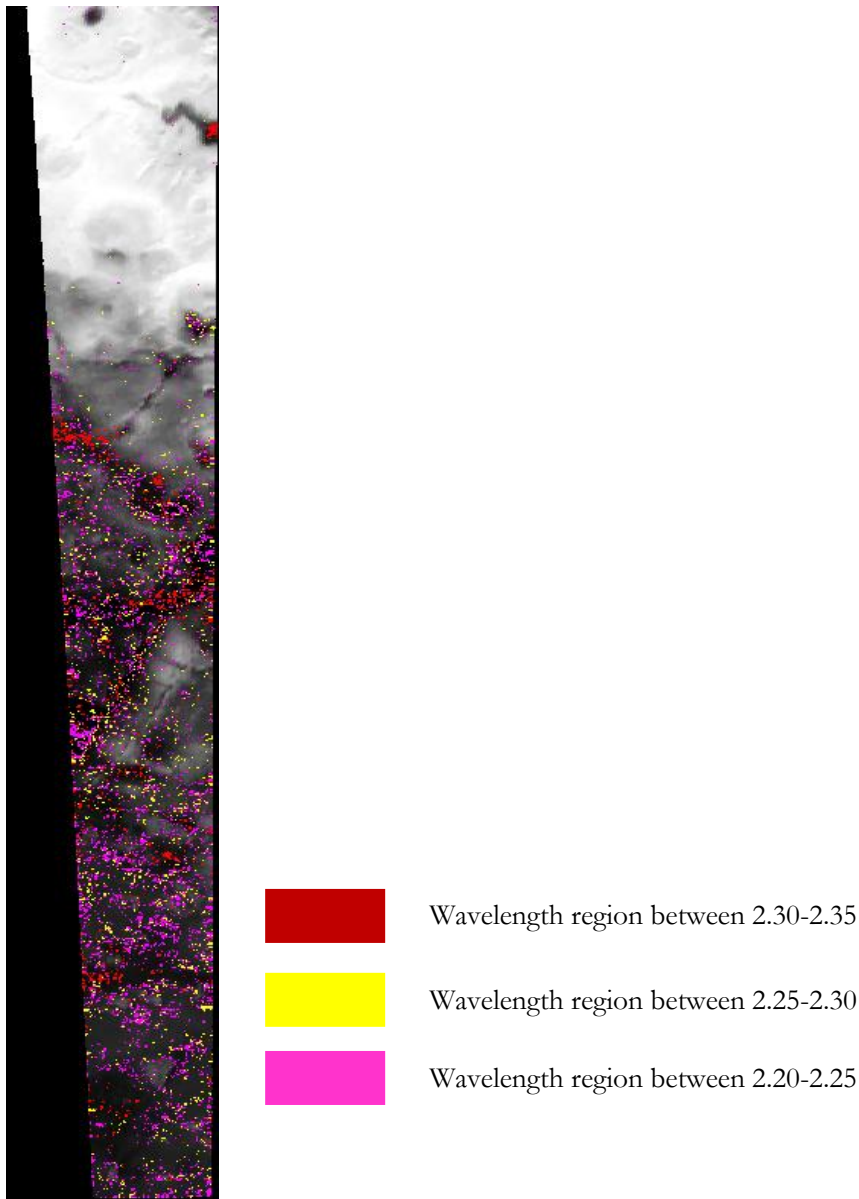
Figure 4-2: ROI of the different wavelength regions draped over the reflectance image from OMEGA image (ORB0232-2)

4.2. Results of comparison of spectra of OMEGA image(ORB0232-2) with library spectra

In this section the results of the comparison between the spectra of ROI of each wavelength region with library spectra have been discussed below.

1. The visual spectral comparison between the spectra of the wavelength regions 2.300-2.350 μm (shown as orange color on Figure 4-1(a)) of the absolute reflectance image and library spectra of some minerals taken from the look up table has been done. Figure4 shows the result of spectral matching of the spectra of this ROI. The result of spectral comparison shows that the absorption features at 1.9 μm and 2.314 μm are similar to the spectra of minerals. Figure 4-3 shows the ROI of the wavelength regions draped over OMEGA (ORB0232-2) image.
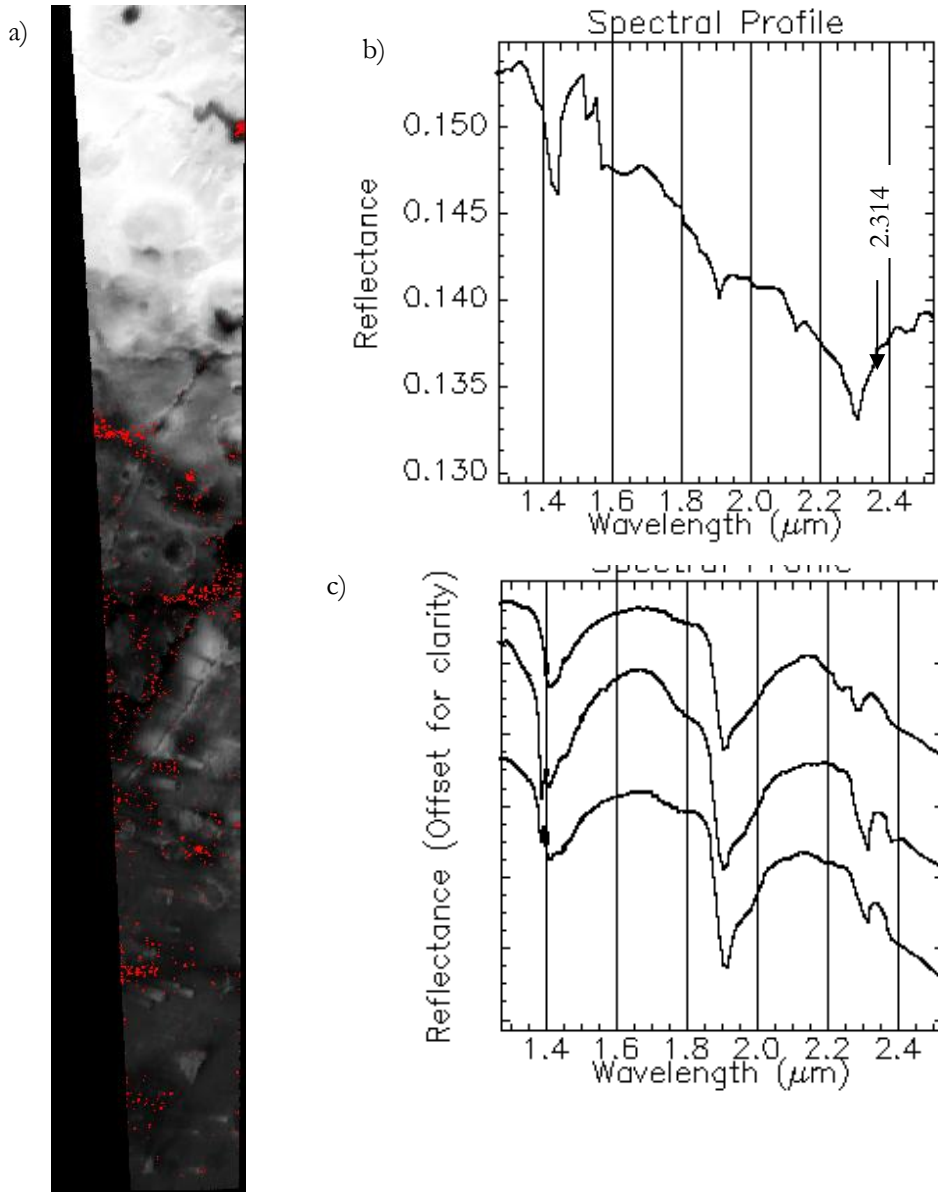
Figure 4-3: (a) ROI of the wavelength range between 2.300-2.320 μm draped over the reflectance image from OMEGA image (ORB0232-2) (b) Mean spectra of the ROI of the wavelength range 2.300-2.350 μm of OMEGA image (ORB0232-2) (c) Spectra of saponite, sepiolite and nontronite from the USGS spectral library

2. The visual spectral comparison of the ROI the wavelength region between 2.250-2.300μm (shown as yellow color on Figure 4-1(a)) of the absolute reflectance image (band 2.314) and library spectra of some mineral has been done. Figure 4-4 shows the result of spectral comparison of the spectra of this wavelength region with library spectra. The result of spectral matching shows that the absorption features of the spectra of the ROI which is at 2.273 μm does not fit with the absorption features of any of the three minerals and it is concluded that there could be a mixture of spectra of different or unknown minerals and also noise in this wavelength

region. Figure 4-4(a) shows the ROI of the wavelength regions draped over OMEGA (ORB0232-2) absolute reflectance image.

a)

b)

c)
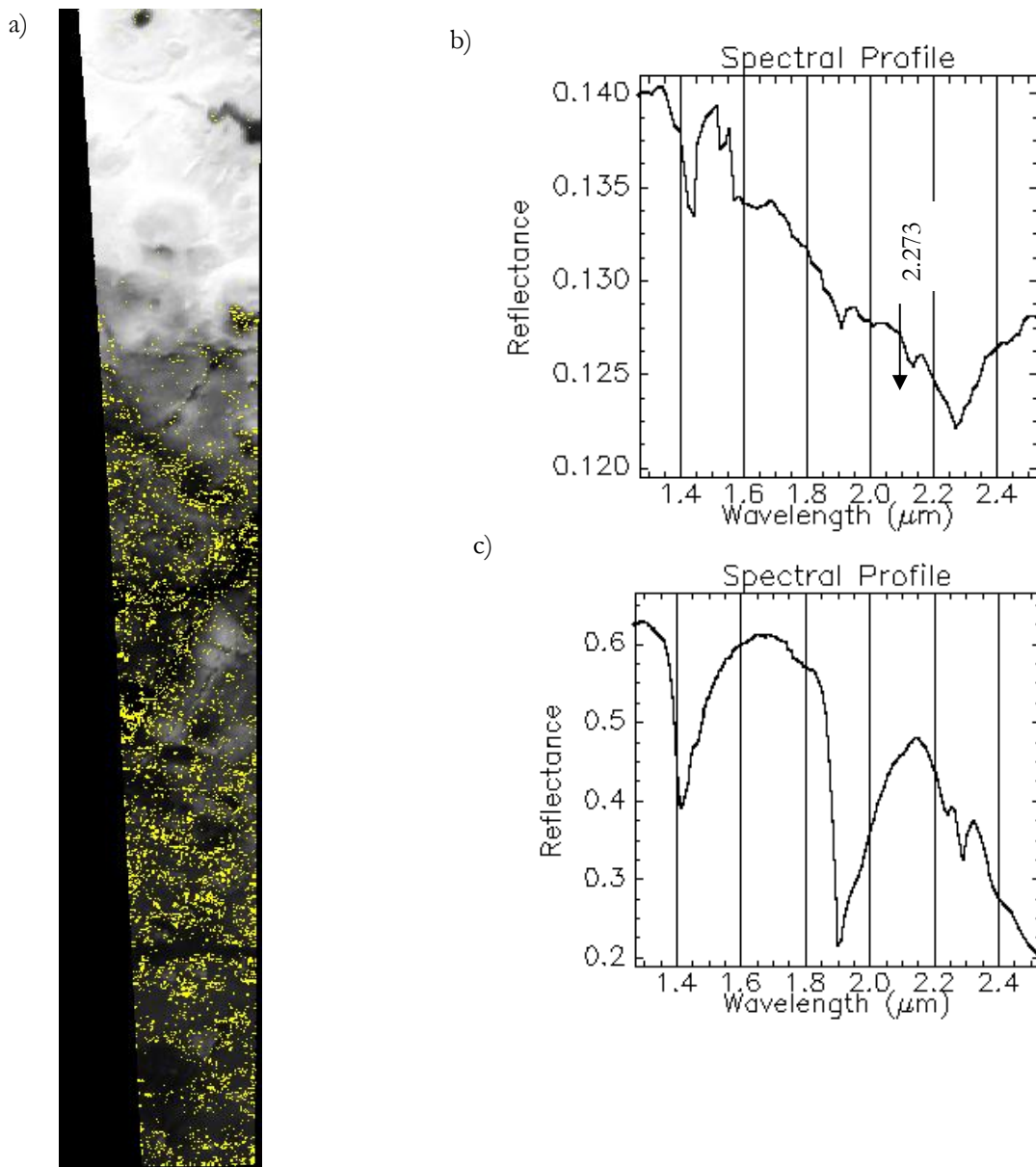
Figure 4-4: (a) ROI of the wavelength region 2.250-2.300 µm draped over the reflectance image from OMEGA (ORB0232-2) image (ORB0232-2) , (b) Mean spectra of the ROI of the wavelength region 2.250-2.290 µm of OMEGA (ORB0232-2) image) and (c) Spectra of nontronite from the USGS spectral library

3. The visual spectral comparison between the ROI of the wavelength region 2.200-2.250 µm (shown as green color on Figure 4-1(a)) of the absolute reflectance image and library spectra of minerals has been done. Figure 4-5 shows the result of spectral matching of the spectra of this ROI. The result of spectral matching shows that the feature at 1.9 µm is similar to kaolinite and montmorillonite. Concerning the absorption feature of kaolinite, montmorillonite and muscovite (2.200, 2.200 and 2.220 µm respectively) is near to the spectra of the ROI of OMEGA image (2.218 µm) and thus it is concluded that kaolinite, montmorillonite and muscovite could be the probable minerals. Figure 4-2 shows all the ROI of the different wavelength regions draped over OMEGA image (ORB0232-2).

a)

b)

c)
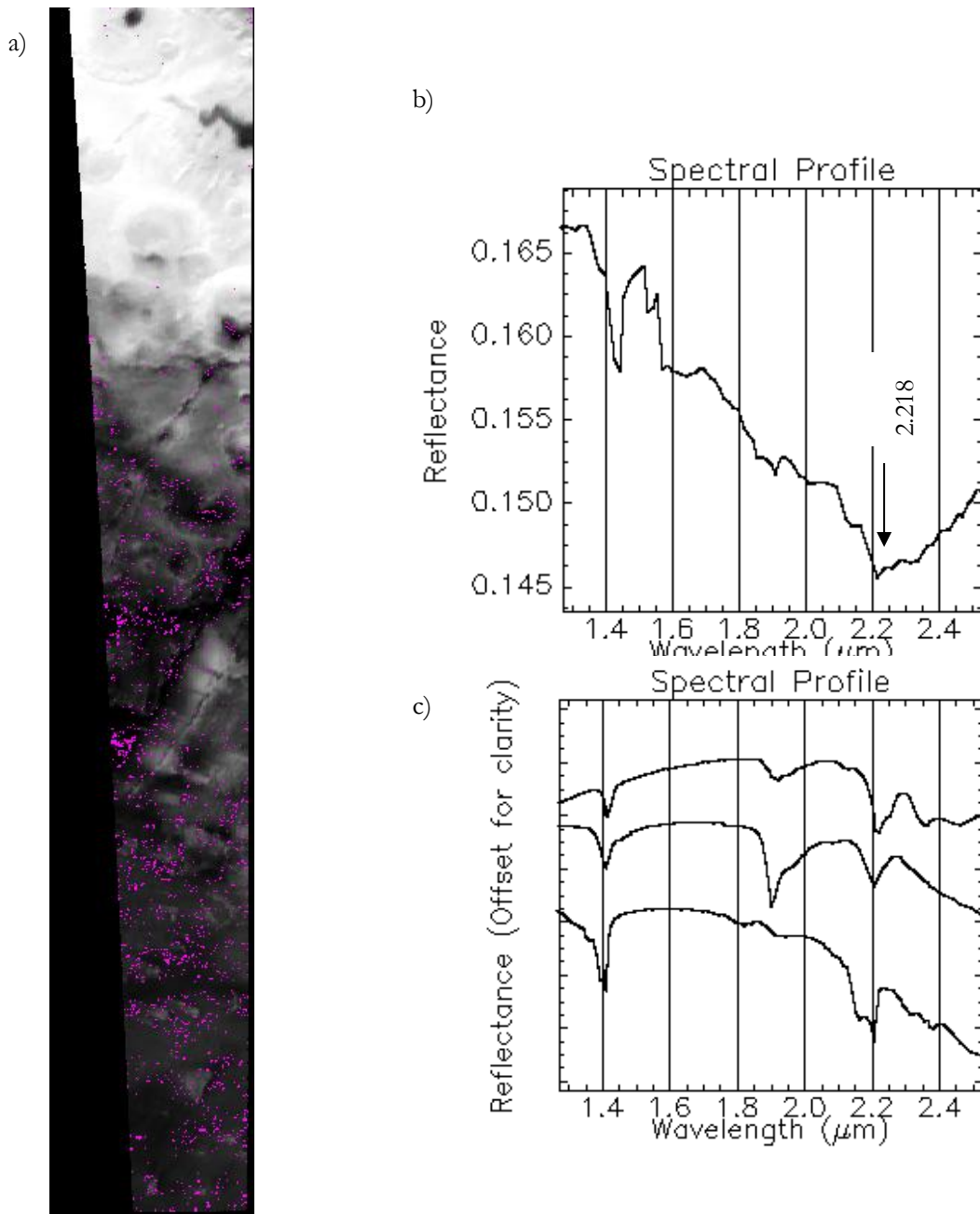
Figure 4-5: (a) ROI of the wavelength region 2.200-2.240 µm draped over reflectance image from OMEGA image (ORB0232-2), (b) Mean spectra of the ROI of the wavelength region 2.190-2.240 µm of OMEGA (ORB0232-2) imagery (ORB0232-2) and (c) Spectra of kaolinite, montmorillonite and muscovite from the USGS spectral library

In general the major part of the mineral distribution of the study area is reflected in the wavelength region 2.30-2.350 µm (shown as orange color on Figure 4-1(a)) of the wavelength map.

4.3.   Results of comparison of spectra of OMEGA image (ORB0232-2) with MOLA data

The stratigraphic sequence of the mineral groups has been observed by draping the wavelength map over the geomorphologic map and also by making stereo images and also 3D view map using wavelength map and MOLA data (Figure 4-6(b)). Thus as observed from the comparison with the geomorphologic and the 3D view

map of the wavelength map, the stratigraphic section of the minerals identified in the different wavelength regions of OMEGA image (ORB0232-2) has been interpreted. Thus the results (Figure 13) shows that the minerals identified in the wavelength region 2.200-2.250 μm (shown as green on Figure 4-6(a)) are dominantly found on the walls of graben and craters. On the other hand the minerals which are identified from the wavelength region 2.300-2.350 μm (shown as orange on Figure 4-6(a)) are found at the floors of craters and graben.
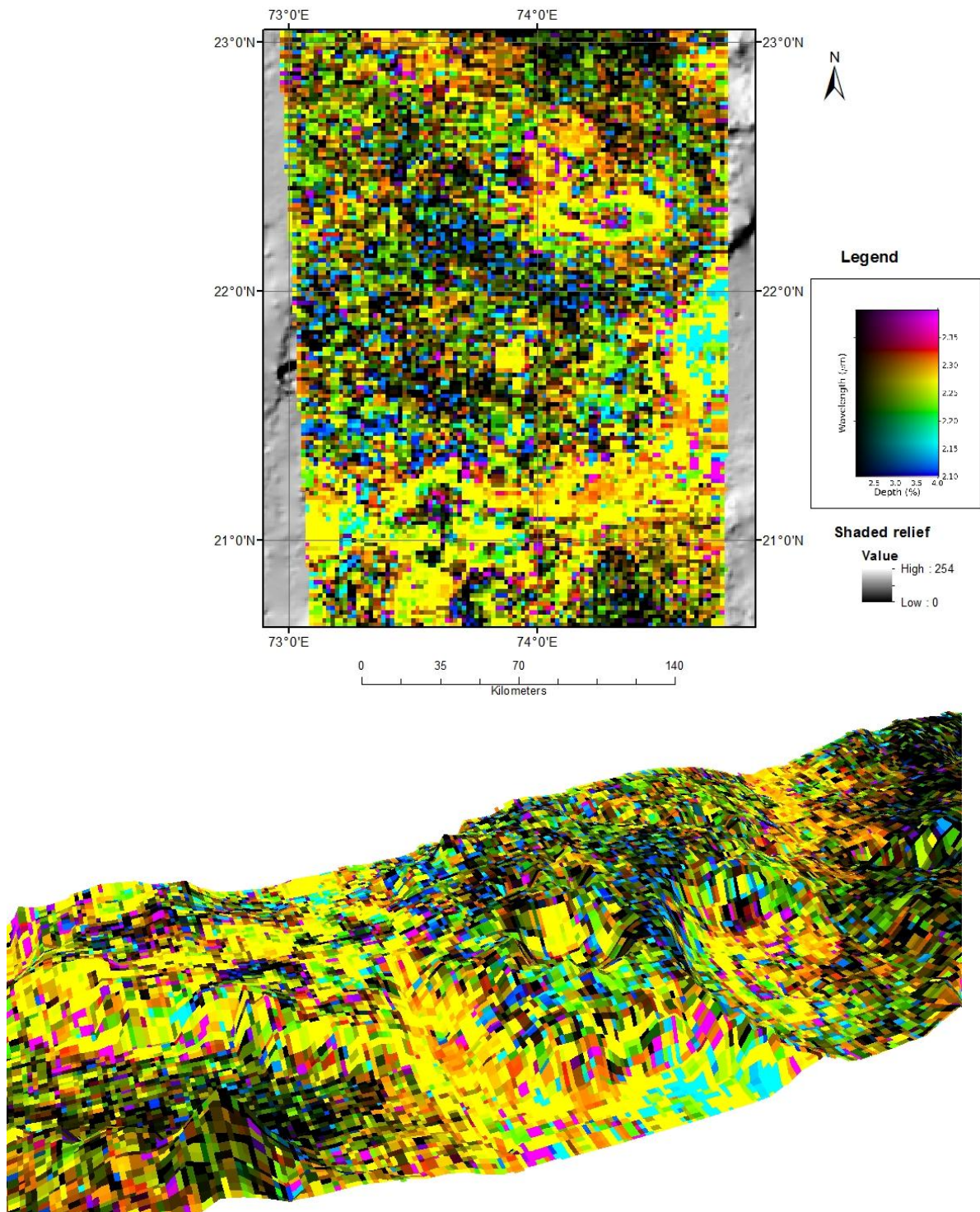
Figure 4-6: (a) Part of the wavelength map of OMEGA image (ORB0232-2) draped over MOLA data and (b) 3D view of part of the study area

4.4.   Results of comparison of spectra of OMEGA image(ORB0232-2) with CRISM images

The comparison between the spectra of OMEGA (ORB0232-2) and CRISM images has been done. In this section the results of the cross validation of OMEGA (ORB0232-2) with CRISM images is discussed. For cross validating with OMEGA (ORB0232-2) image three CRISM images have been selected keeping in mind that comparison incorporates two issues:

-To validate the results of the comparison between OMEGA (ORB0232-2) with library spectra. At this point part of the OMEGA (ORB0232-2) image which shows clear spectra has been chosen to be compared with CRISM image.

-To validate the results of draping the wavelength map from OMEGA (ORB0232-2)image over the 3D view of MOLA data of the study area. At this point part of the OMEGA (ORB0232-2) image which is found in a specific geomorphologic unit has been chosen to be compared with CRISM images.

For the sake of simplicity three CRISM images have been taken on different parts of the study area taking in to consideration the overlap with this OMEGA (ORB0232-2) image scene and with different geomorphologic units in different parts of the study area. Due to this, locations at rims of craters, walls of craters and graben and floors of craters and graben have been chosen for cross validation between OMEGA (ORB0232-2) and CRISM images. In addition it has been focused to validate those wavelength regions which gave clear spectral features while comparing with library spectra. In addition the three wavelength ranges will be validated using CRISM image.

The ROI of the three CRISM image have been created following the procedures discussed in section 3.8. Before the comparison made between the two images, each ROI of CRISM image has been reconciled to OMEGA image (ORB0232-2) and intersected with the ROI of OMEGA image. The comparison between the different ROI of each wavelength range of CRISM image with OMEGA image (ORB0232-2) has been discussed in detail below.
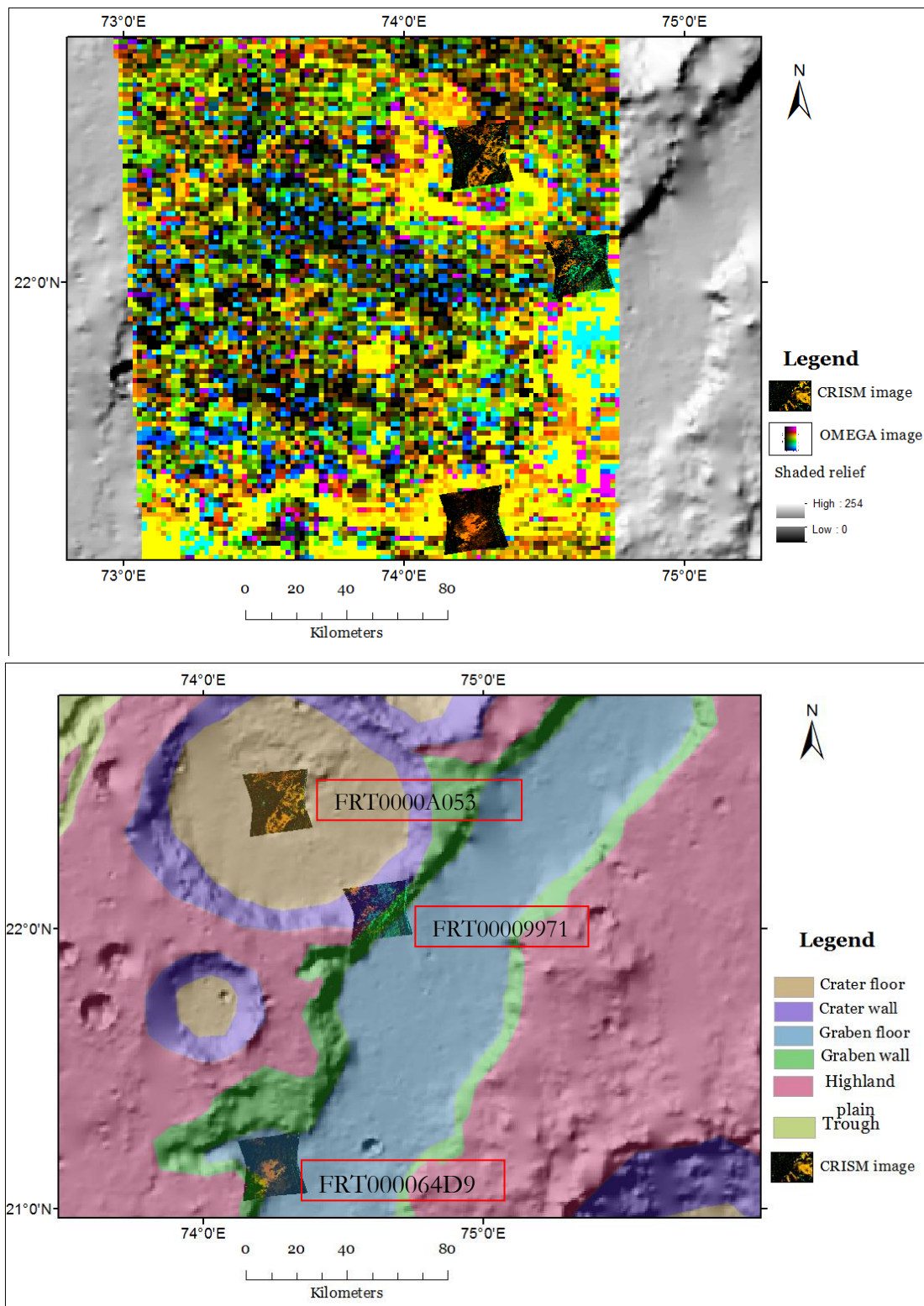
Figure 4-7: The location of the three CRISM image (b) on wavelength map of OMEGA image (ORB0232-2) (b) on geomorphologic map

4.5.   Results of comparison of OMEGA image(ORB0232-2) with CRISM image(FRT0000A053)

Before the comparison has been made between the ROI of CRISM and ROI of OMEGA image (ORB0232-2) in the wavelength range between 2.300-2.350 μm, the ROI of CRISM (FRT0000A053) image (386976pixels) has been reconciled to ROI of OMEGA (ORB0232-2) image (1355 pixels) to intersect and get pixels at their common location. And then the mean spectrum of the ROI of OMEGA image (ORB0232-2) at the common location of the two images (9 pixels) has been computed in order to compare with the mean spectrum of the ROI of CRISM (FRT0000A053) image.

The result of comparison between the spectra of ROI of CRISM image (FRT0000A053) and ROI of OMEGA (ORB0232-2) imagery shows that both spectra have similar absorption features at 1.9 μm which indicates the presence of water molecule (H_2O). On the other hand, the spectrum of the OMEGA image spectra shows absorption features at 2.300 μm while CRISM image (FRT0000A053) shows at 2.314 μm. Figure 4-9 shows the comparison between the spectra of the two images in the wavelength range between 2.300-2.350 μm. From this result it is concluded that CRISM image validates what has been observed from MEGA (ORB0232-2) at the center of the crater and thus the minerals identified on CRISM image (FRT0000A053) could also be found on OMEGA image (ORB0232-2). Figure 4-8 shows the ROI of the two images draped over the reflectance image of their respective images.

a)

b)

Figure 4-8: (a) OMEGA image draped with ROI of OMEGA(ORB0232-2 and CRISM(FRT0000A053) images (b) CRISM image (FRT0000A053) draped with the ROI of CRISM in the wavelength range between 2.300-2.350 μm

a) Spectra of ROI of OMEGA image in the wavelength range 2.300-2.350 µm

b) Spectra of ROI of CRISM image in the wavelength range 2.300-2.350 µm

Figure 4-9: Visual comparison of (a) mean spectra of ROI of OMEGA image (ORB0232-2) and (b) mean spectra of ROI of CRISM image (FRT0000A053) in the wavelength range between 2.300-2.350 µm

4.6. Results of validation of OMEGA(ORB0232-2) with CRISM (FRT00009971) images

Before the comparison has been made between the spectra of ROI of CRISM and ROI of OMEGA (ORB0232-2) images in the wavelength range between 2.200-2.240 µm, the ROI of CRISM (FRT0000A053) image (2778 pixels) has been reconciled to ROI of OMEGA (ORB0232-2) image (4515 pixels) to intersect and get the pixels at their common location. And then the mean spectrum of the ROI of OMEGA image (ORB0232-2) at the common location of the two images (11 pixels) has been computed in order to compare with the mean spectrum of the ROI of CRISM (FRT0000A053) image. Figure 4-11 shows the spectral comparison of the two images.

The result of comparison between the spectra of ROI of CRISM image (FRT0000A053) and ROI of OMEGA (ORB0232-2) imagery shows that the spectrum of CRISM image (FRT0000A053) shows absorption features at 2.200 while that of OMEGA (ORB0232-2) image shows at 2.234 µm. The 1.9 feature has been observed only on spectra of OMEGA image (ORB0232-2). The other features of CRISM image (FRT0000A053) 1.659, 1.9,

2.200, 2.3906 and 2.483 µm. Figure 4-10 shows the ROI of OMEGA (ORB0232-2) and CRISM ((FRT0000A053) images draped over their respective absolute reflectance image.

Thus it is concluded that the spectra of the ROI of CRISM image (FRT0000A053) does not validate OMEGA image.
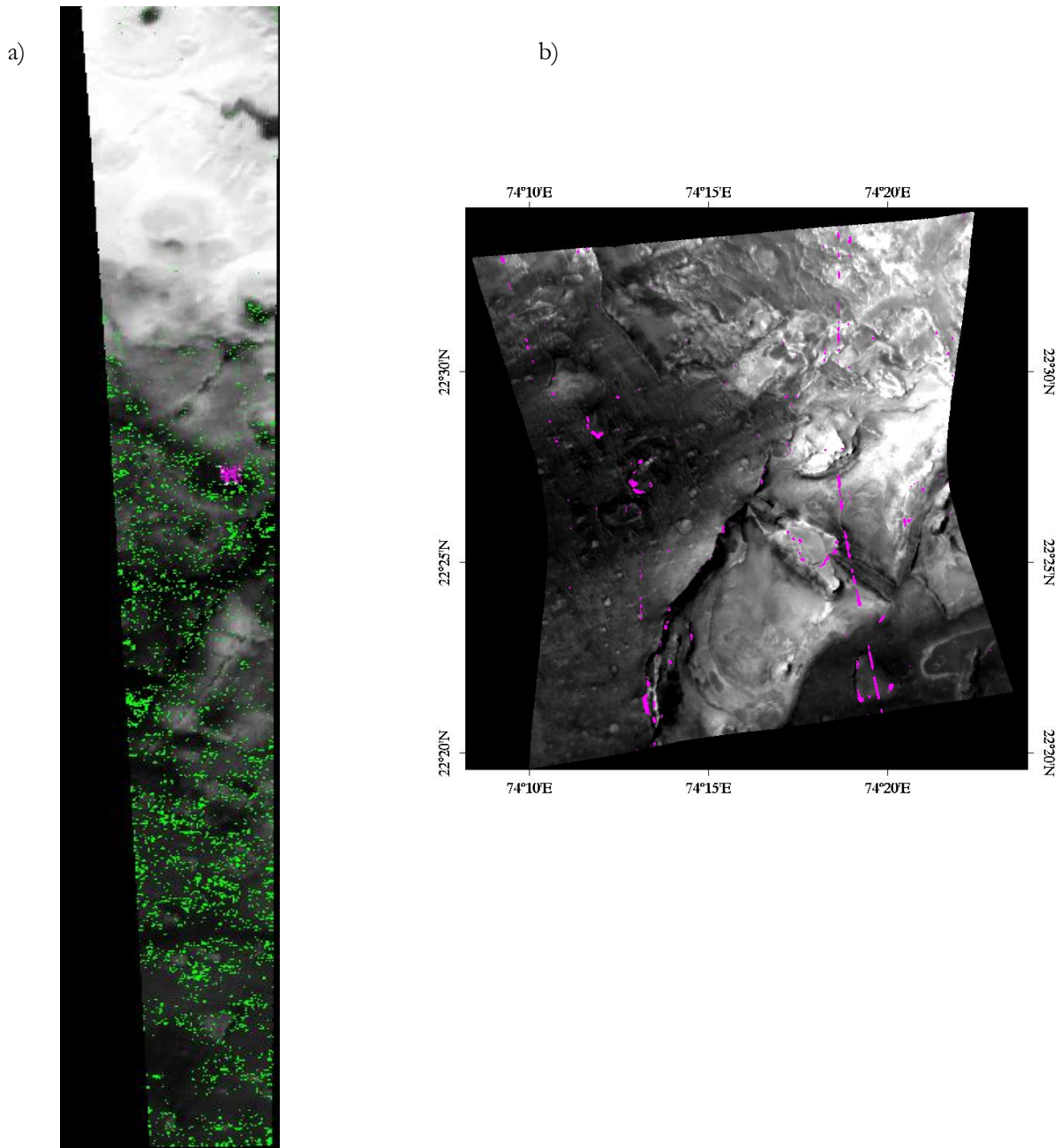
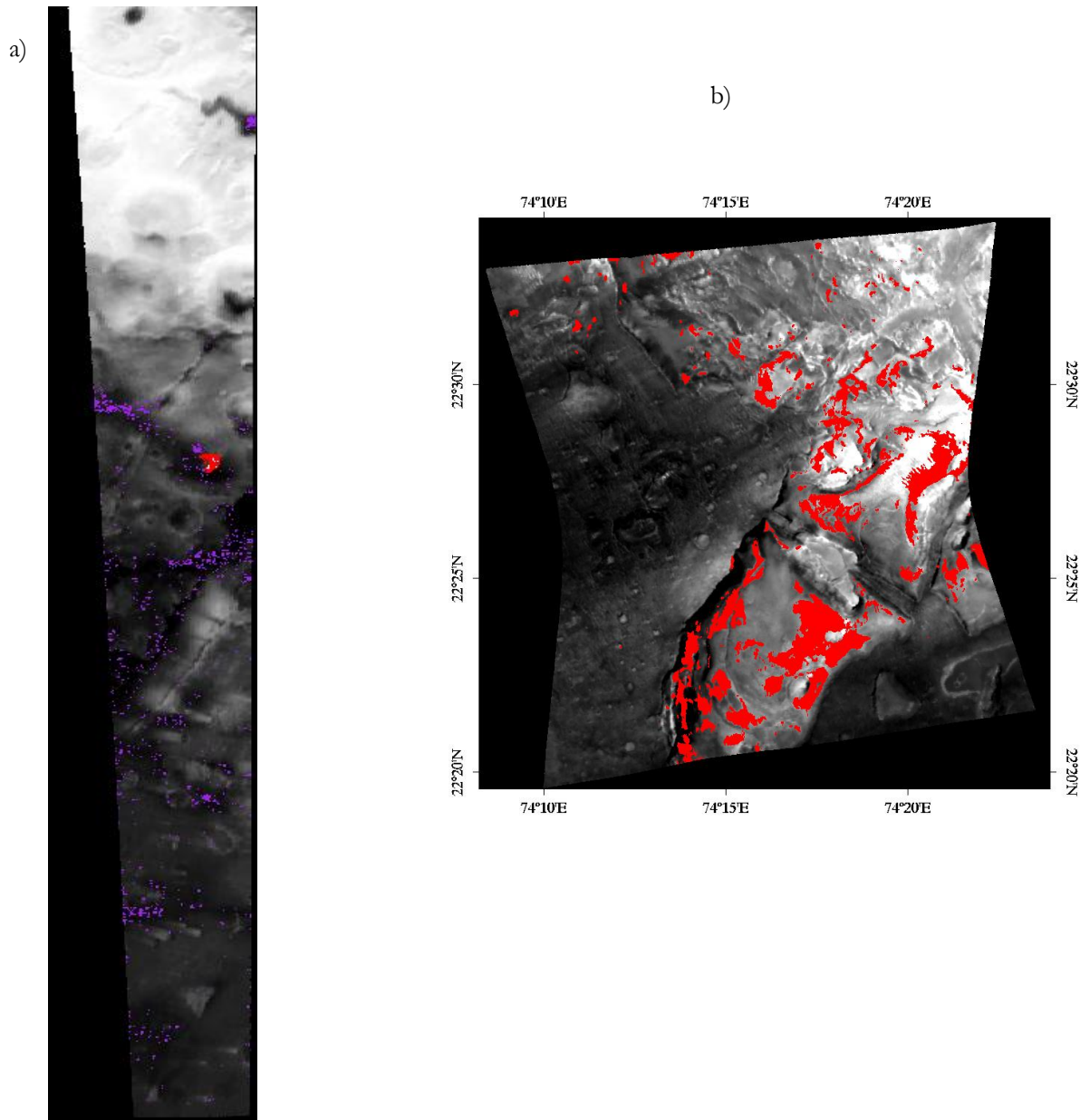
Figure 4-10: a) OMEGA image draped with the ROI of OMEGA and CRISM images (b) CRISM image (FRT0000A053) draped with the ROI of the wavelength range between 2.200-2.2240 µm of CRISM image

a) Spectral Profile

Mean spectra of ROI of OMEGA image in the wavelength range 2.200-2.240 µm

b) Spectral Profile

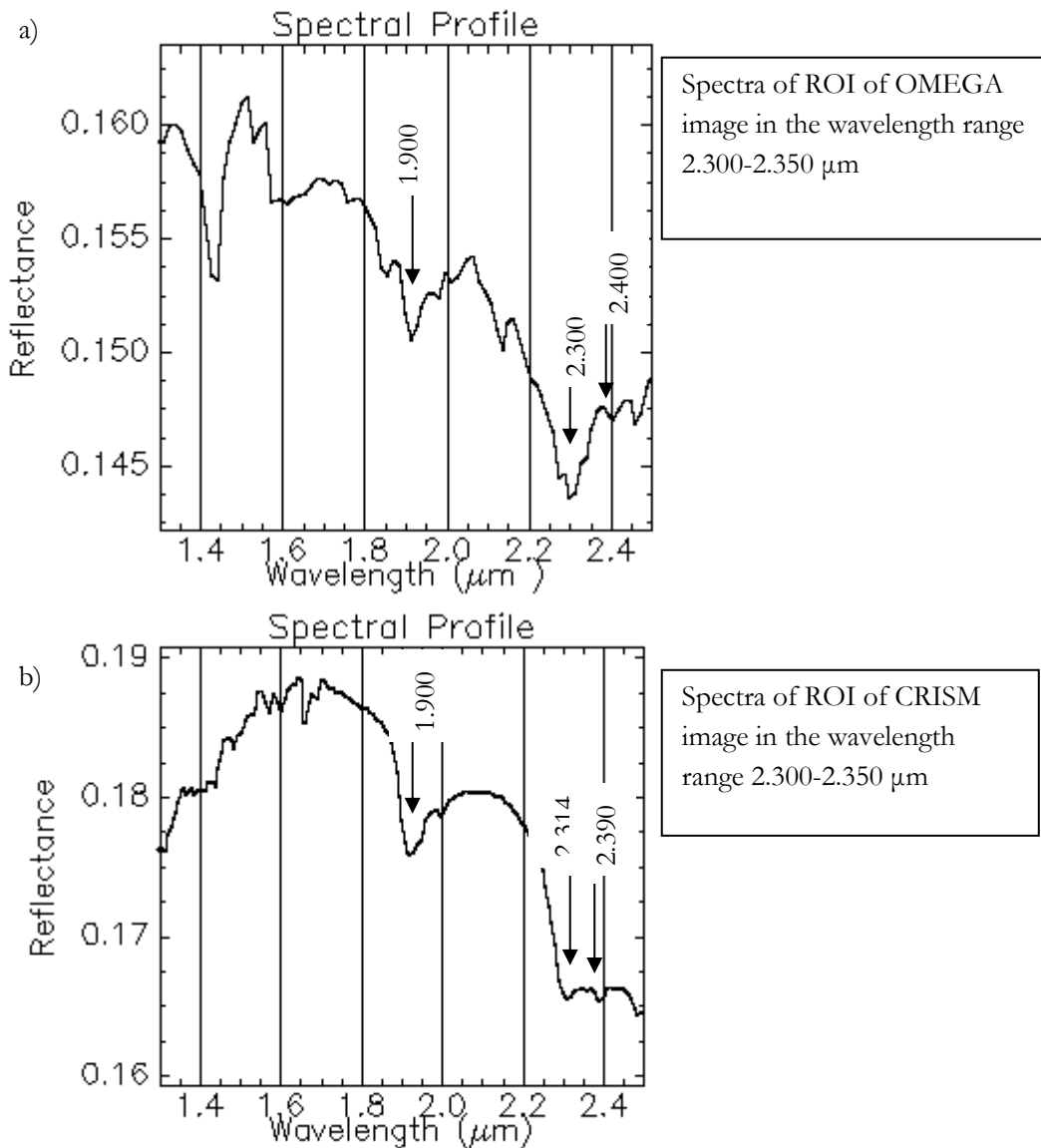Mean spectra of ROI of CRISM image in the wavelength range 2.200-2.240 µm

Figure 4-11: Comparison of (a) mean spectra of ROI of OMEGA image (ORB0232-2) and (b) mean spectra of ROI of CRISM image (FRT0000A053) in the wavelength range between 2.200-2.240 µm

4.7.   Results of validation of OMEGA (ORB0232-2) with CRISM (FRT00009971) images

Before the comparison has been made between the ROI of CRISM (FRT00009971) and ROI of OMEGA (ORB0232-2) images in the wavelength range between 2.300-2.350 µm, the ROI of CRISM (FRT00009971) image (8629 pixels) has been reconciled to ROI of OMEGA (ORB0232-2) image (1355 pixels) to intersect and get the pixels at their common location. And then the mean spectrum of the ROI of OMEGA image (ORB0232-2) at the common location of the two images (4 pixels) has been computed in order to compare with the mean spectrum of the ROI of CRISM (FRT00009971)) image. Figure 4-14 shows the spectral comparison of the two images.

The result of the visual spectral comparison shows that the spectra of the ROI of OMEGA (ORB0232-2) and CRISM images (FRT00009971) have common feature at 1.9 µm. On the other hand the spectra of the ROI of OMEGA image (ORB0232-2) shows absorption feature at 2.136 and 2.314 µm while that of CRISM image (FRT00009971) shows at 2.312 µm. The other features which are found only on the spectra of the ROI of OMEGA (ORB0232-2) image the feature at 1.4 which is missing on CRISM spectra On the other hand a spectrum of ROI of CRISM (FRT00009971) shows features at 2.390 µm and 2.483 µm which are not found on

spectra of ROI of OMEGA (ORB0232-2) image. From the cross validation between OMEGA (ORB0232-2) and CRISM images it is concluded that the CRISM image validates what has been observes from OMEGA image at the center of the crater. Figure 4-12 shows the ROI of OMEGA (ORB0232-2) and CRISM ((FRT00009971images draped over their respective absolute reflectance image.

Thus it is concluded that the spectra of the ROI of CRISM image (FRT00009971) validates the ROI of OMEGA in the wavelength range between 2.200-2.240µm based on the deepest absorption which has been observed on the spectra of both images (at 2.314µm).

Figure 4-12: (a) OMEGA image draped with the ROI of OMEGA and CRISM images (b) CRISM image (FRT00009971)) draped with the ROI of CRISM image in the wavelength range between 2.300-2.350 µm

Figure 4-13: Comparison of (a) mean spectra of ROI of OMEGA image (ORB0232-2) and (b) mean spectra of ROI of CRISM image (FRT00009971) in the wavelength range between 2.300-2.350µm

Before the comparison has been made between the ROI of CRISM (FRT00009971) and ROI of OMEGA image (ORB0232-2) in the wavelength range between 2.200-2.240 µm, the ROI of CRISM (FRT00009971) image (18714 pixels) has been reconciled to ROI of OMEGA (ORB0232-2) image (2344 pixels) to intersect and get the pixels at their common location. And then the mean spectrum of the ROI of OMEGA image (ORB0232-2) at the common location of the two images (10 pixels) has been computed in order to compare with the mean spectrum of the ROI of CRISM (FRT00009971) image. Figure 4-16 shows the spectral comparison of the two images.

The result of comparison between the ROI of CRISM (FRT00009971) image and ROI of OMEGA (ORB0232-2) image in the wavelength range 2.200-2.240 µm shows that both spectra have common feature at 1.9. On the other hand the spectra of the ROI of OMEGA (ORB0232-2) image shows absorption feature at 2.218 µm while the spectra of the ROI of CRISM image shows absorption feature at 2.198 µm and it is concluded that CRISM image validates what has been observed from OMEGA image at the edge of the crater and graben(Figure). The other features observed on the spectra of the two images are the 1.4 µm feature on OMEGA (ORB0232-2) spectra which is missing on CRISM spectra and the 2.390 µm and 2.483 µm features on CRISM spectra which

are not observed on OMEGA (ORB0232-2) spectra. Figure 4-15 shows the ROI of OMEGA (ORB0232-2) and CRISM (FRT00009971) images draped over their respective absolute reflectance image.

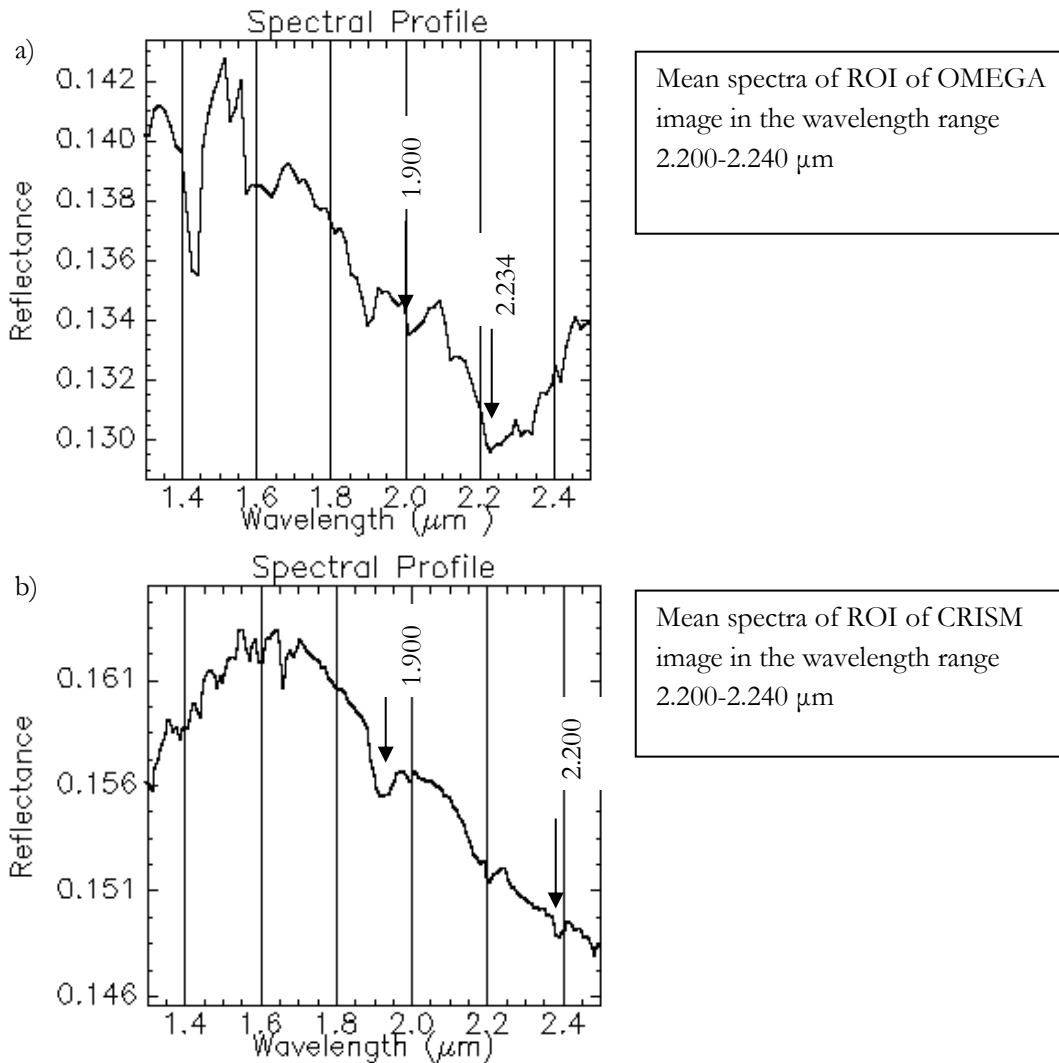Thus it is concluded that the spectra of the ROI of CRISM image (FRT00009971) validates the ROI of OMEGA in the wavelength range between 2.200-2.240 μm based on the deepest absorption which has been observed on the spectra of both images (2.200- 2.2180 μm).
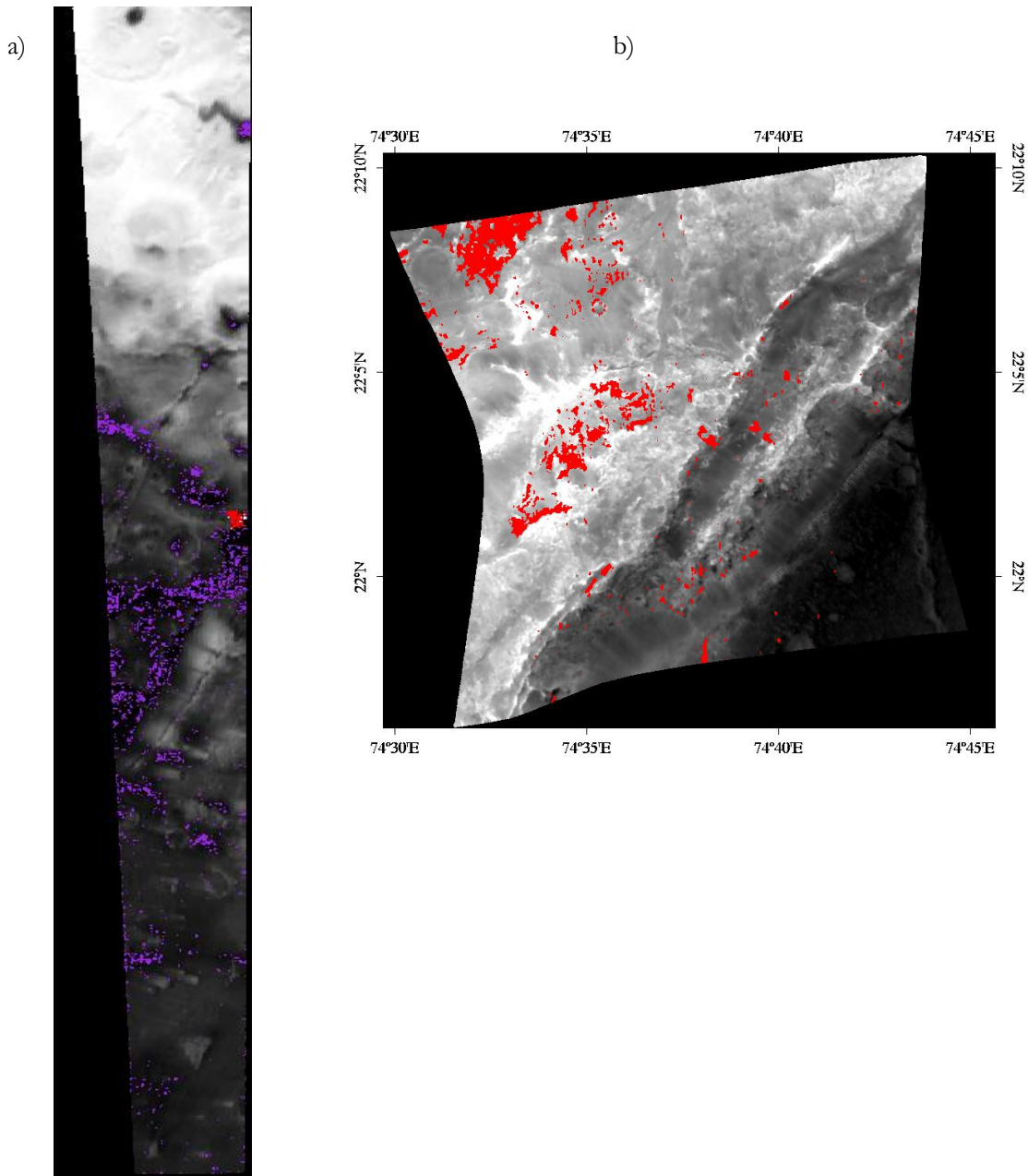

Figure 4-14: OMEGA (ORB0232-2) image draped with the ROI of OMEGA and CRISM images (b) CRISM image (FRT00009971) draped with ROI of the image wavelength range between 2.200-2.240 μm

a) Mean spectra of ROI of OMEGA image in the wavelength range 2.200-2.240 µm

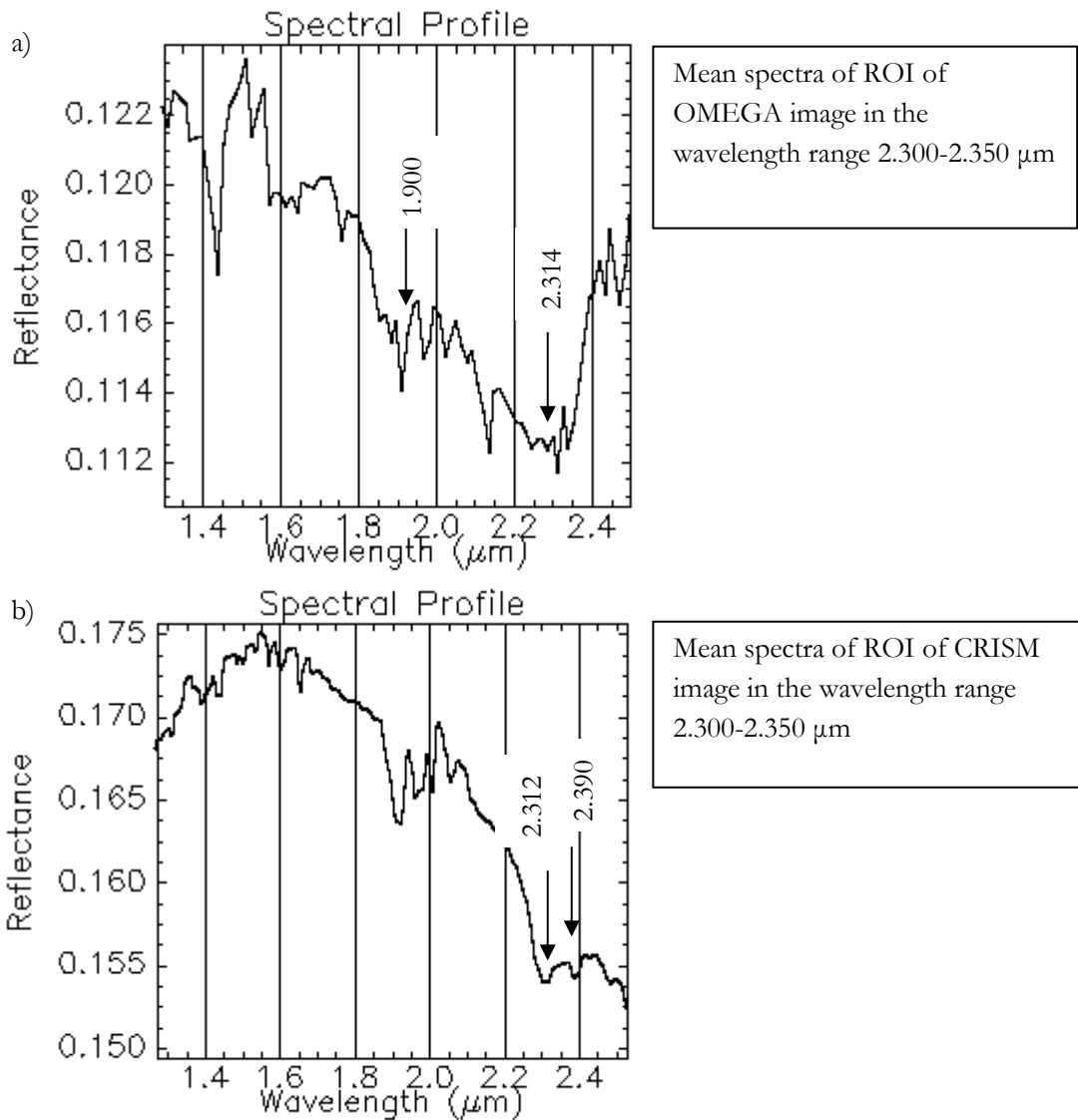b) Mean spectra of ROI of CRISM image in the wavelength range 2.200-2.240 µm

Figure 4-15: Comparison of (a) mean spectra of ROI of OMEGA image (ORB0232-2) and (b) mean spectra of ROI of CRISM image (FRT00009971) in the wavelength range between 2.200-2.240 µm

4.8. Results of validation between OMEGA (ORB0232-2) and CRISM (FRT000064D9) images

Before the comparison has been made between the ROI of CRISM (FRT000064D9) and ROI of OMEGA image(ORB0232-2), in the wavelength range between 2.300-2.350 µm, the ROI of CRISM image (FRT000064D9) (22347 pixels) has been reconciled to ROI of OMEGA (ORB0232-2) image (1355 pixels) to intersect and get the pixels of OMEGA image at their common location. And then the mean spectrum of the ROI of OMEGA image (ORB0232-2) at the common location of the two images (4 pixels) has been computed in order to compare with the mean spectrum of the ROI of CRISM (FRT000064D9) image. Figure 4-17 shows the spectral comparison of the two images.

The result shows that the spectra of the ROI of OMEGA image (ORB0232-2) shows absorption feature at 2.314 µm and spectra of CRISM image (FRT000064D9) shows absorption feature at 2.317 µm. Based on this deepest absorption feature of the two images, it is concluded that this CRISM image validates what has been observed on OMEGA image at the floor of the graben. Thus it is concluded that the spectra of the ROI of CRISM image validates the ROI of OMEGA in the wavelength range between 2.300-2.350µm based on the deepest absorption

which has been observed on the spectra of both images (at 2.314μm). Figure 4-16 shows the ROI of OMEGA (ORB0232-2) and CRISM (FRT000064D9) draped over their respective absolute reflectance image.
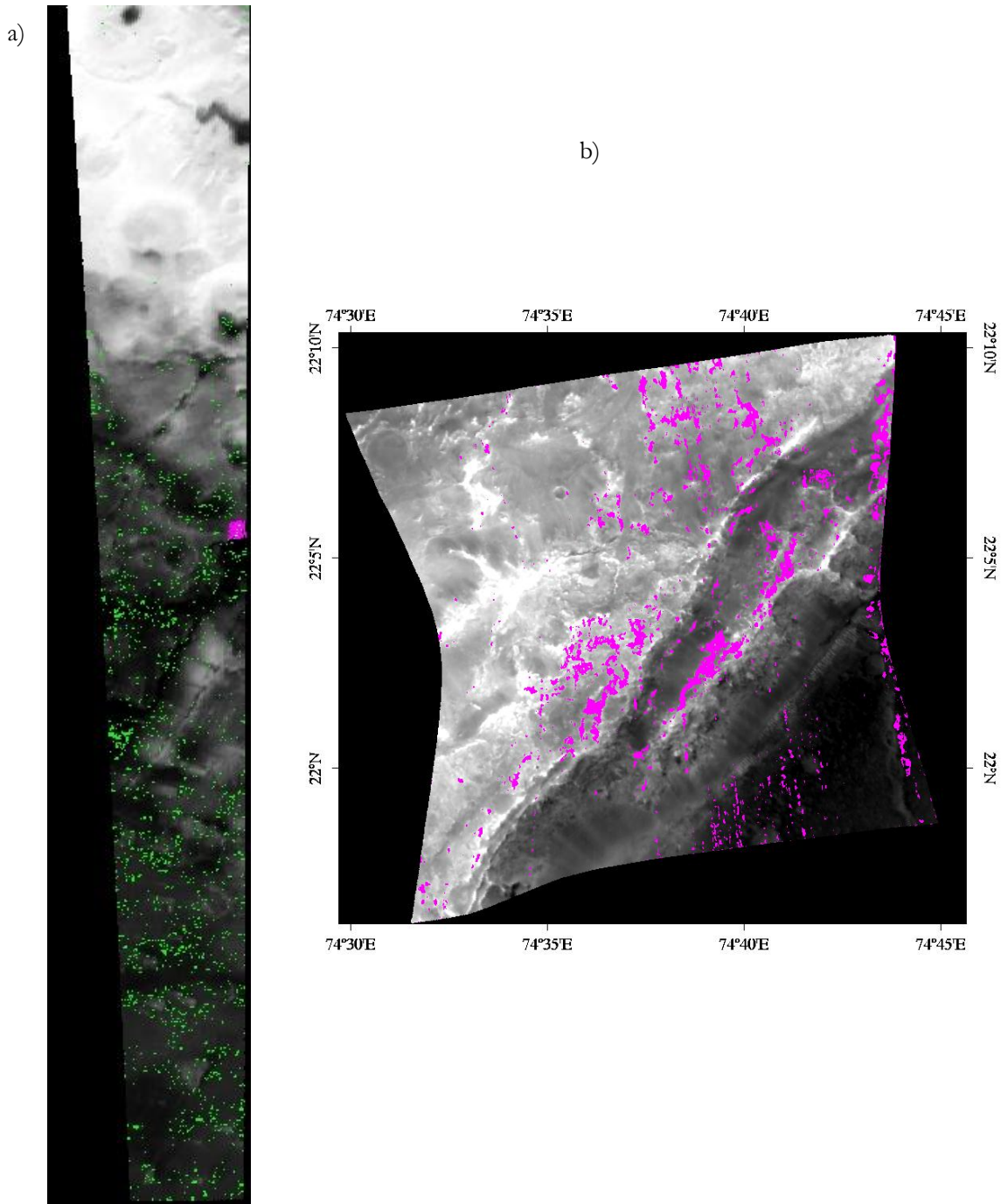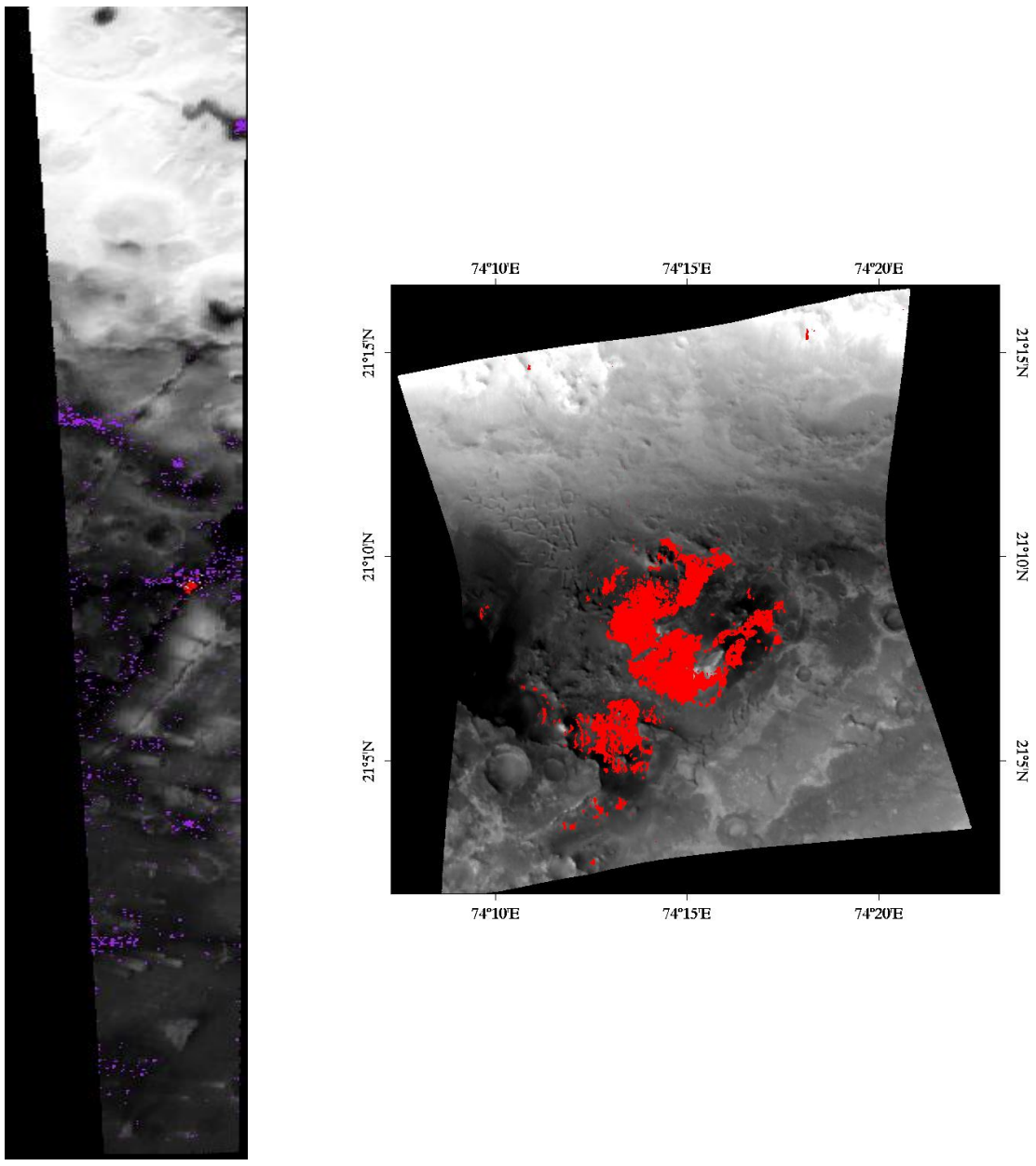

Figure 4-16: (a) OMEGA image draped with the ROI of OMEGA and CRISM images (b) CRISM image (FRT000064D91) draped with ROI of the wavelength range between 2.300-2.350 μm
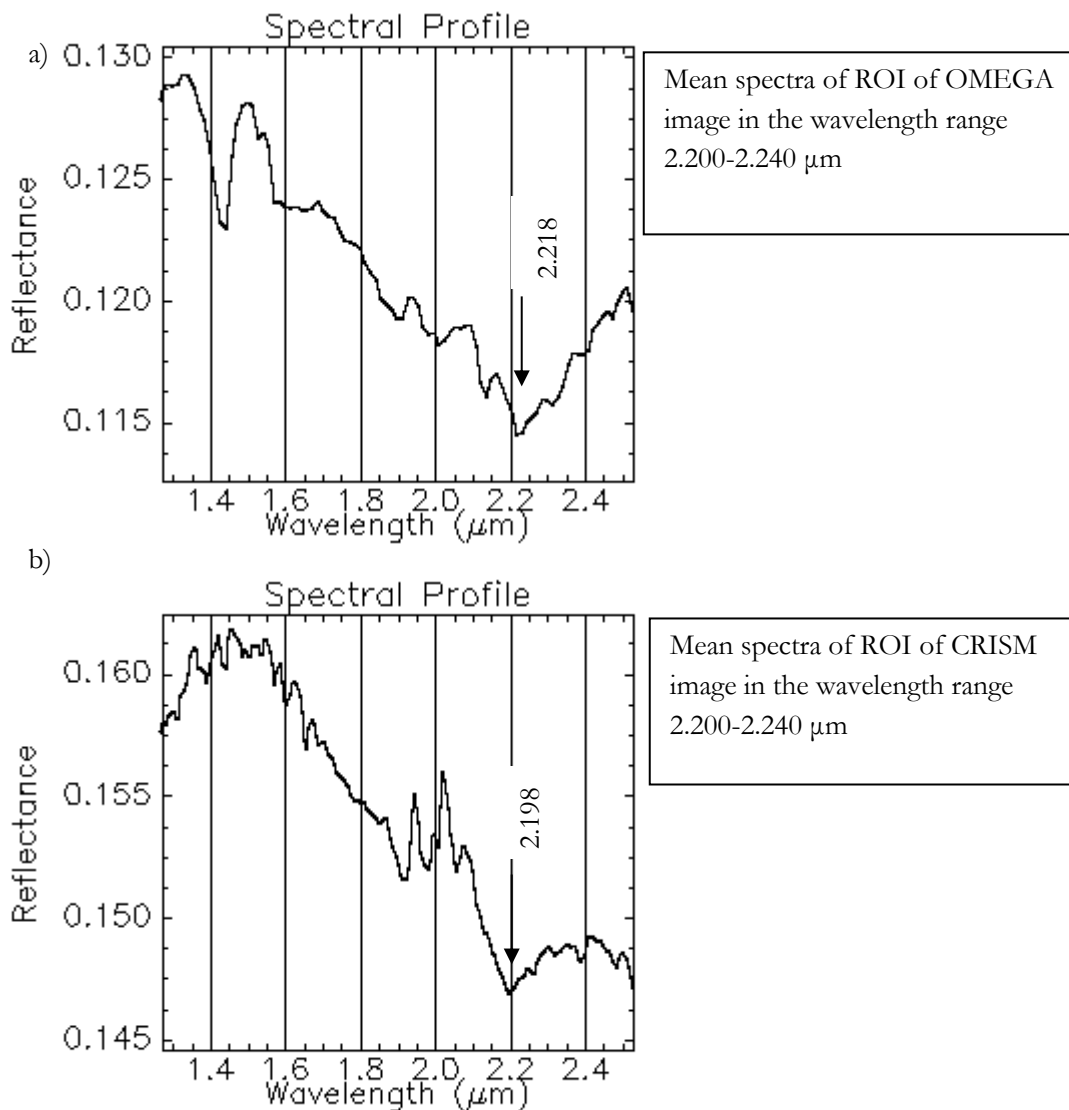
a) Mean spectra of ROI of OMEGA image in the wavelength range 2.300-2.350 µm

b) Mean spectra of ROI of CRISM image in the wavelength range 2.300-2.350 µm
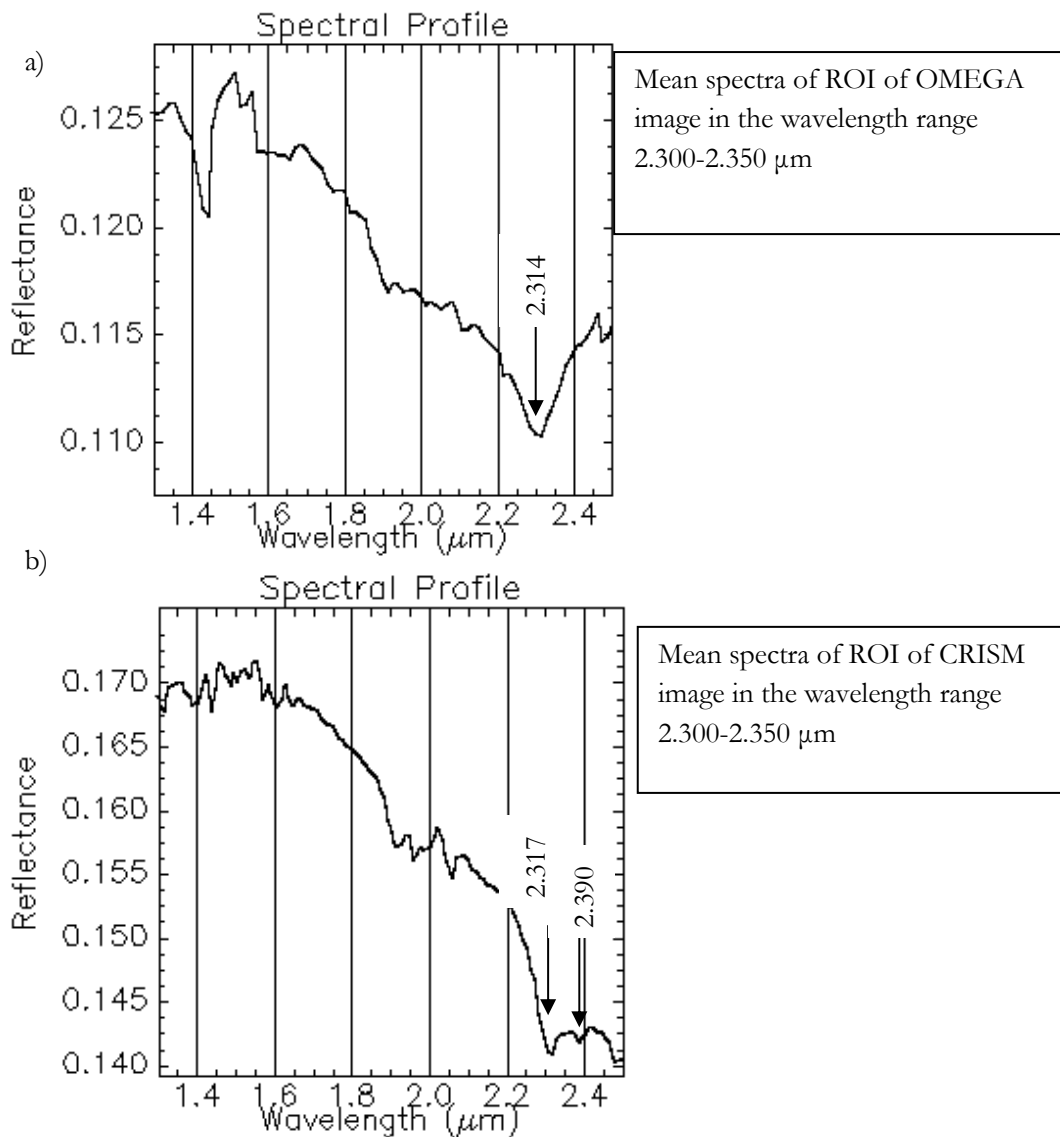
Figure 4-17: Comparison of (a) mean spectra of ROI of OMEGA image (ORB0232-2) and (b) mean spectra of ROI of CRISM image (FRT000064D9)

The other wavelength ranges of the CRISM image (FRT000064D91) has not been considered because they do not have common pixels with OMEGA image (ORB0232-2).

4.9.   Results of stratigraphic validationbetween OMEGA (ORB0232-2) and CRISM images

The result shows that the stratigraphic section of the wavelength region 2.20-2.25 µm part of the wavelength map which has been interpreted to represent kaolinite and montmorillonite mineral groups has been found above the stratigraphic section. The stratigraphic section of the wavelength region 2.30-2.35 µm of the wavelength map which have been interpreted to represent saponite and sepiolite mineral groups have been found at the bottom of the stratigraphic section.

The result of the comparison between CRISM image and MOLA data confirmed the stratigraphic sequence of the minerals which has been observed from comparison of OMEGA image (ORB0232-2) with geomorphologic

map of the study area and MOLA data. Thus result shows the kaolinite group of minerals the above the Fe-Mg silicate minerals on CRISM (FRT00009971) and CRISM (FRT0000A053) images which are found at the edge of the crater and the graben and at the center of the crater . In addition the same stratigraphic section has been observed from the CRISM (FRT0000A053) image which is found at the center of the crater which is found at the North West part of the study area.

5.   DISCUSSION

The main objective of this research was to prove the applicability of wavelength mapping method for interpretation of OMEGA imagery for identification of surface minerals of Nili Fossae area. To achieve this goal OMEGA data has been preprocessed and the wavelength mapping method has been applied in order to interpret the data. The wavelength map gives spectral information about the presence of certain minerals by showing the wavelength position of the deepest absorption feature in wavelength regions between 2.1 and 2.4 µm on a pixel-by-pixel basis. And then the reflectance spectra of the same pixels were visually compared with library spectra to identify minerals. Draping of the wavelength map over the geomorphologic map has been done in order to explore the relationship between the position of the absorption features and geomorphologic units. In places where vertical mineral zonation were exposed the stratigraphy of the minerals in the study area was studied. Finally a comparison was made between OMEGA and CRISM images and also with results of other researchers in order to validate the results of OMEGA image spectra. The advantage of wavelength mapping method in combination with creating Regions of Interest (ROI) was minimizing of the noise and the artifacts present in OMEGA image and enable to get better spectra to identify minerals. In order to achieve the main objective and facilitate the subsequent discussion, the following sections discuss the output of the work with emphasis on specific objectives and the subsequent research questions formulated during this research.

5.1.   Comparing spectra of OMEGA image(ORB0232-2) with the USGS library spectra

In this study, OMEGA imagery was analyzed and compared with spectra of the USGS spectral library to identify minerals in the study area. The comparison between OMEGA and library spectra resulted in a list of candidate minerals that could be present in the study area. These minerals include saponite and sepiolite with clear deepest absorption feature at 2.314 µm, and kaolinite and montmorillonite with deepest absorption feature at 2.218 µm.

5.2.   3D view of the wavelength map of OMEGA image(ORB0232-2) draped over the MOLA data

The 3D visualization of the wavelength map and the MOLA data has been investigated as mentioned in section 4.3. The stratigraphy of the minerals which have been observed on walls and floors of craters and graben showed that the kaolinite group of minerals overlays the saponite group of minerals.

CRISM image of the eastern part of Nili Fossae region evidenced that the Fe/Mg smectite-bearing rocks are the bottom of the stratigraphic section (Mangold et al., 2007a; Mustard et al., 2008; Mustard et al., 2007). Ehlmann et al., mentioned the exposure of smectite-bearing basement rocks from 72E to 80E at the walls of the Nili Fossae trough. Moreover the authors indicated that the kaolinite bearing rocks overlies two types of Fe/mg smectites-bearing deposits: massive crustal smectites as well as layered sedimentary smectites. The stratigraphy occurred on the other hand Mustard et al., (2009) discussed the existence of small exposure of kaolinite bearing material which are exposed by erosion.

The excavation of hydrous phases by the process of impact craters have been observed repeatedly which is restricted to the Noachian terrain of Mars(Bibring et al., 2005b)In the central peak area of a crater in the Nili Fossae region hydration signatures on OMEGA spectra have been reported by Mangold et al.,(2007).

5.3. Comparison between OMEGA (ORB0232-2) and CRISM imagery

The CRISM imagery used in this study showed spectral similarity with OMEGA image in the wavelength ranges 2.20-2.25 and 2.30-2.35 μm in different parts of the study area as mentioned in section 4.9. The CRISM image spectra show absorptions features which resemble certain minerals which are expected in the study area. Thus the spectra of the CRISM images (FRT00009971) and (FRT0000A053) and images show clear evidence of the absorption feature at 2.314 μm and the 2.218 μm which is also observed in the spectra of OMEGA image. In addition the spectra of the CRISM image (FRT000064D91 μm) also show the absorption feature at 2.314 but does but it does not common location with range 2.20-2.25 of OMEGA image so it was not compared with OMEGA image.

Wavelength mapping method is applicable for mineralogical interpretation of OMEGA imagery in Nili Fossae area and this has been proved from comparison which has been made between OMEG with library spectra (Figure 5-1). In addition the cross validation between OMEGA and CRISM shows that the two images are correlated and gives a clue on the interpretable nature of OMEGA imagery for mineral identification.
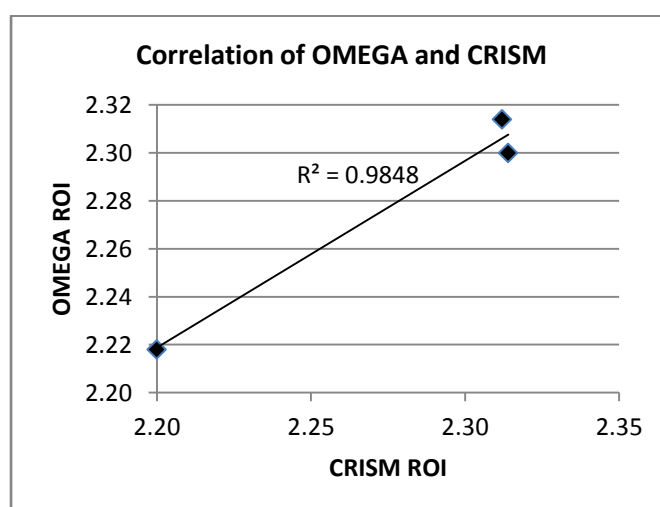
Figure 5-1: Correlation between the ROI of OMEGA (ORB0232-2) and CRISM images (FRT00009971 and FRT0000A053)

The result of this comparison between OMEGA and CRISM images has been strongly evidenced by the work of Ehlmann et al., 2008 which inferred the 2.3-2.31 μm features are that of Fe-Mg smectites and the features at 2.2 μm to that of kaolinite and montmorillonite. They explained by referring the works of (Mangold et al, 2007; Mustard et al, 2007, 2008). She mentioned in her paper that the area from 72E TO 80E, the smectite-bearing basement rock is well exposed by erosion in numerous locations, including in a 600 m thick section of the walls of the trough.

And these results have correlation with what Ehlmann et al., (2008) discussed about the Noachian highland of Nili Fossae area dominantly covered by phyllosilicates and the phyllosilicates are Fe-Mg smectites and also Al-smectites. On the other hand the cross validation of OMEGA and CRISM shows the stratigraphic sequence of the area in similar way with other researchers (e.g. Ehlmann, etc.).

Furthermore the stratigraphic sequence of the minerals identified has been also shown clearly in CRISM image which confirms the result of OEMGA image. In addition the stratigraphic sequence of the minerals has been also evidenced by the work of Ehlmann et al. (2008).

5.4. General discussion

This research illustrated the applicability of the wavelength mapping method to interpret OMEGA imagery for identifying surface minerals of the Nili Fossae region of Mars. This research tried to address the problems associated with OMEGA imagery which make the data difficult to interpret. To overcome these obstacles the wavelength mapping method has been applied. Different preprocessing steps were applied on OMEGA imagery which helps to clean up the noise and other artifacts. The results showed and confirmed that the OMEGA image is interpretable for mineral identification using wavelength mapping method. In addition the interpretation of wavelength map of OMEGA imagery has been validated by the results of interpretation of CRISM images of the study area. In general the applicability of wavelength mapping method for interpreting OMEGA imagery is demonstrated by comparing the results from the interpretation with literatures. For instance the Fe-Mg silicates have been identified from OMEGA image interpretation using spectral comparison with laboratory spectra at wavelength range between 2.3-2.4 µm in Nili Fossae region. The minerals saponite and sepiolite are the possible minerals identified in the region and this has been shown by the results in section 4.2. Furthermore, Al-silicates have been identified from OMEGA imagery by spectral comparison with laboratory spectra of earth materials. In the wavelength region between 2.0-2.2 µm montmorillonite and kaolinite group of minerals have been identified (section 4.2).

The main idea is that in most cases the wavelength range 2.3-2.5 µm is clearly seen in the wavelength maps of OMEGA and CRISM imagery than the other ranges and this could be due to the shallowness of the depth of the absorption features of the minerals which could indirectly covered by dust particles and noise from different sources. The second reason could be the minerals existing in the study area are dominantly found in this wavelength region and also their spectra depth is higher than the others which helped not to be covered by dust particles and other sources of noise.

It is concluded that OMEGA imagery contains spectral information that is to some extent reproducible by the higher resolution CRISM imagery. This shows that OMEGA provides information about the surface mineralogy of Mars on a regional scale. And since the focus of this research was confined to the SWIR of the electromagnetic radiation and this range is most applicable for mapping of minerals the minerals which are identified are on the range between 2-2.5 µm and thus the minerals found are alteration minerals of phyllosilicates which incorporates Fe-Mg silicates and Al-silicate minerals so from this it can be inferred that the reason for the presence of hydrated minerals on Mars could be due to different processes which have interaction with water like hydrothermal alteration, impact processes, weathering processes and so on. And this was mentioned in the paper of Ehlmann et al. (2008) that the phyllosilicates which are found on Mars are found only in the Noachian terrains and are exposed by erosion or impact (Poulet, 2005). Moreover the 1.4 feature is common feature on spectra of OMEGA image and it could be related to calibration problem. On the other hand a 1.6 mm feature is common and clearly seen on the CRISM image spectra which are not seen in OMEGA imagery.

Fe/Mg smectites have been detected using OMEGA image with absorption feature near to 2.3 µm and a 1.9 µm band indicating H_2O in Nili Fossae region (Mangold et al., 2007a; Poulet et al., 2005). Ehlmann et al.,(2008) explained that the even if the strength of the 1.9 µm feature is affected by the degree of hydration, the position of this feature does not show variation among the Fe/Mg smectites due to this it does not give any informational composition.

Ehlmann et al. (2008) identified kaolinite from the spectra of CRISM images of Nili Fossae region with absorption features at 1.4 and 2.2 µm. Mustard et al., 2009 mentioned the existence of phyllosilicates in the walls of Nili Fossae region and they are dominated by chlorite and saponite with minor amounts of nontronite, Al-smectite kaolinite and other minerals (Ehlmann et al., 2008b) and these minerals are exposed in many impact craters.

6.   CONCLUSIONS AND RECOMMENDATIONS

6.1.   CONCLUSIONS

In this research the applicability of wavelength mapping method for interpreting OMEGA imagery for surface mineral identification of Nili Fossae region of Mars was studied. A lot of preprocessing techniques have been applied on OMEGA image before further analysis has been performed on OMEGA imagery. The wavelength mapping method helped to get wavelength map which contains wavelength regions representing spectra of different minerals with their absorption depth. The wavelength map has been used to create Region of Interest (ROI) which represents each wavelength region. The research questions (section 1.4) and the research findings in this research are presented below.

Research Question 1: What information can be extracted by comparing the spectra retrieved from OMEGA imagery with spectral libraries of USGS?

The comparison between the spectra of the OMEGA imagery with library spectra of USGS identified the minerals saponite and sepiolite in the wavelength region between 2.30-2.35 and kaolinite and montmorillonite in the wavelength region between 2.20-2.25. But there is no any mineral identified in the wavelength region 2.25-2.30 and this could be related to the random noise distributed over the image and also mixture of unknown minerals in this wavelength region.

Research Question 2: What can we extract by draping the wavelength map from OMEGA imagery 3D view of MOLA data and geomorphologic map?

The wavelength map has been draped over 3D map and also geomorphologic map of the study area to visualize the stratigraphy of the minerals identified from the comparison between OMEGA image and library spectra of USGS helped to observe the stratigraphic sequence of the minerals identified kaolinite and montmorillonite overlying the saponite and sepiolite minerals in impact craters. In addition the stratigraphy has been observed in crater floors, crater walls, crater rim, and graben walls.

Research Question 3: What can we conclude by comparing OMEGA with that of CRISM imagery?

The comparison between the spectra extracted from OMEGA and that of CRISM images confirmed the spectra of the minerals identified from OMEGA imagery. Thus it is concluded that absorption features of the spectra of OMEGA image in the wavelength region 2.300-2.350 are correlated with that of CRISM image and thus it is concluded that the minerals are representing Fe-mg smectites which could be observed in spectra of OMEGA image. In addition the absorption features of the spectra of the wavelength region between 2.200-2.240 are correlated with kaolinite and montmorillonite and thus it is concluded that these minerals are representing the kaolinite group of minerals which have been observed in OMEGA image spectra.

Research Question 4: What can we conclude by comparing the results of the research with the results of other researches?

The results of the research have been compared with results from other researchers and it is concluded that the research correlates with what has been found previously. For instance in the research kaolinite and

montmorillonite have been identified and these minerals are also identified by other researches in the Nili Fossae region. As same time saponite and sepiolite are identified in this research and other researches also detected this in the study area.

Research Question 4: Is wavelength mapping method applicable for mineralogical interpretation of OMEGA imagery in Nili Fossae region of Mars?

Based on the results obtained from the analysis done on the applicability of wavelength mapping method it is concluded that wavelength mapping method is applicable for interpreting OMEGA imagery of Mars for mineral identification of the Nili Fossae region of Mars.

6.2. RECOMMENDATIONS

Based on the results obtained and the limitations of this research, recommendations are given.

- Further work has to be done on improving the noise filtering mechanisms of OMEGA imagery and also a means of better calibrating the OMEGA images to minimize the different sources of noise
- It is advisable to apply wavelength mapping method to other parts of Mars for mineral interpretation purpose. And also it would be better if other methods are integrated with it.
- It is very important if the research is accompanied with ground trothing.

LIST OF REFERENCES

Bakker, W. H., van Ruitenbeek, F. J. A., and van der Werff, H. M. A., 2009, Processing omega hyperspectral imagery for mineral mapping of the Nili Fossae area on Mars : abstract + powerpoint: Presented at Geological mapping of Mars : a workshop on new concepts and tools, 12-14 October 2009, Il Ciocco, Italy. 45 p.

Bandfield, J. L., 2002, Global mineral distributions on Mars: J. Geophys. Res., v. 107.

Bibring, J.-P., Langevin, Y., Gendrin, A., Gondet, B., Poulet, F., Berthé, M., Soufflot, A., Arvidson, R., Mangold, N., Mustard, J., Drossart, P., and team, t. O., 2005a, Mars Surface Diversity as Revealed by the OMEGA/Mars Express Observations: Science, v. 307, no. 5715, p. 1576-1581.

Bibring, J. P., 2005, Mars surface diversity as revealed by the OMEGA/Mars Express observations: Science, v. 307, p. 1576-1581.

Bibring, J. P., Langevin, Y., Gendrin, A., Gondet, B., Poulet, F., Berthé, M., Soufflot, A., Arvidson, R., Mangold, N., Mustard, J., and Drossart, P., and team, t. O., 2005b, Mars Surface Diversity as Revealed by the OMEGA/Mars Express Observations: Science, , v. 307, no. 5715, p. 1576-1581.

Bibring, J. P., Langevin, Y., Mustard, J. F., Poulet, F., Arvidson, R., Gendrin, A., Gondet, B., Mangold, N., Pinet, P., Forget, F., and team, O., 2006, Global mineralogical and aqueous mars history derived from OMEGA/Mars express data: Science, v. 312, no. 5772, p. 400-404.

Bishop, J., Madejova, J., Komadel, P., and Froschl, H., 2002, The influence of structural Fe, Al and Mg on the infrared OH bands in spectra of dioctahedral smectites: Clay Miner., v. 37, p. 607-616.

Daswani, M. M., 2011, Mineral spectra extraction and analysis of the surface mineralogy of Mars with hyperspectral remote sensing,MSc Thesis]: University of Twente Faculty of Geo-Information and Earth Observation (ITC), 62 p.

Ehlmann, B. L., 2009, Identification of hydrated silicate minerals on Mars using MRO-CRISM: geologic context near Nili Fossae and implications for aqueous alteration: J. Geophys. Res., v. 114, p. E00D08.

Ehlmann, B. L., Mustard, J. F., Fassett, C. I., Schon, S. C., Head Iii, J. W., Des Marais, D. J., Grant, J. A., and Murchie, S. L., 2008a, Clay minerals in delta deposits and organic preservation potential on Mars: Nature Geosci, v. 1, no. 6, p. 355-358.

Ehlmann, B. L., Mustard, J. F., and Murchie, S. L., 2010, Geologic setting of serpentine deposits on Mars: Geophys. Res. Lett., v. 37, no. 6, p. L06201.

Ehlmann, B. L., Mustard, J. F., Murchie, S. L., Poulet, F., Bishop, J. L., Brown, A. J., Calvin, W. M., Clark, R. N., Marais, D. J., Milliken, R. E., Roach, L. H., Roush, T. L., Swayze, G. A., and Wray, J. J., 2008b, Orbital identification of carbonate-bearing rocks on Mars: Science (New York, N.Y.), v. 322, no. 5909, p. 1828-1832.

Hamilton, V. E., and Christensen, P. R., 2005, Evidence for extensive, olivine-rich bedrock on Mars: Geology, v. 33, p. 433-436.

Hoefen, T. M., Clark, R. N., Bandfield, J. L., Smith, M. D., Pearl, J. C., and Christensen, P. R., 2003, Discovery of Olivine in the Nili Fossae Region of Mars: Science, v. 302, no. 5645, p. 627-630.

Mangold, N., Poulet, F., Mustard, J. F., Bibring, J. P., Gondet, B., Langevin, Y., Ansan, V., Masson, P., Fassett, C., Head, J. W., Hoffmann, H., and Neukum, G., 2007a, Mineralogy of the Nili Fossae region with OMEGA/Mars Express data: 2. Aqueous alteration of the crust: Journal of Geophysical Research-Planets, v. 112, no. E8.

Mangold, N., Poulet, F., Mustard, J. F., Bibring, J. P., Gondet, B., Langevin, Y., Ansan, V., Masson, P., Fassett, C., Head, J. W., III, Hoffmann, H., and Neukum, G., 2007b, Mineralogy of the Nili Fossae region with OMEGA/Mars Express data: 2. Aqueous alteration of the crust: J. Geophys. Res., v. 112, no. E8, p. E08S04.

Murchie, S., Arvidson, R., Bedini, P., Beisser, K., Bibring, J. P., Bishop, J., Boldt, J., Cavender, P., Choo, T., Clancy, R. T., Darlington, E. H., Des Marais, D., Espiritu, R., Fort, D., Green, R., Guinness, E., Hayes, J., Hash, C., Heffernan, K., Hemmler, J., Heyler, G., Humm, D., Hutcheson, J., Izenberg, N., Lee, R., Lees, J., Lohr, D., Malaret, E., Martin, T., McGovern, J. A., McGuire, P., Morris, R., Mustard, J., Pelkey, S., Rhodes, E., Robinson, M., Roush, T., Schaefer, E., Seagrave, G., Seelos, F., Silverglate, P., Slavney, S., Smith, M., Shyong, W. J., Strohbehn, K., Taylor, H., Thompson, P., Tossman, B., Wirzburger, M., and Wolff, M., 2007, Compact Reconnaissance Imaging Spectrometer for Mars (CRISM) on Mars Reconnaissance Orbiter (MRO): J. Geophys. Res., v. 112, no. E5, p. E05S03.

Murchie, S., Kirkland, L., Erard, S., Mustard, J., and Robinson, M., 2000, Near-Infrared Spectral Variations of Martian Surface Materials from ISM Imaging Spectrometer Data: Icarus, v. 147, no. 2, p. 444-471.

Murchie, S. L., Seelos, F. P., Hash, C. D., Humm, D. C., Malaret, E., McGovern, J. A., Choo, T. H., Seelos, K. D., Buczkowski, D. L., Morgan, M. F., Barnouin-Jha, O. S., Nair, H., Taylor, H. W., Patterson, G. W., Harvel, C. A., Mustard, J. F., Arvidson, R. E., McGuire, P., Smith, M. D., Wolff, M. J., Titus, T. N., Bibring, J. P., and Poulet, F., 2009, Compact Reconnaissance Imaging Spectrometer for Mars investigation and data set from the Mars Reconnaissance Orbiter's primary science phase: Journal of Geophysical Research-Planets, v. 114.

Mustard, J. F., Murchie, S. L., Pelkey, S. M., Ehlmann, B. L., Milliken, R. E., Grant, J. A., Bibring, J. P., Poulet, F., Bishop, J., Dobrea, E. N., Roach, L., Seelos, F., Arvidson, R. E., Wiseman, S., Green, R., Hash, C., Humm, D., Malaret, E., McGovern, J. A., Seelos, K., Clancy, T., Clark, R., Marais, D. D., Izenberg, N., Knudson, A., Langevin, Y., Martin, T., McGuire, P., Morris, R., Robinson, M., Roush, T., Smith, M., Swayze, G., Taylor, H., Titus, T., and Wolff, M., 2008, Hydrated silicate minerals on Mars observed by the Mars Reconnaissance Orbiter CRISM instrument: Nature, v. 454, no. 7202, p. 305-309.

Mustard, J. F., Poulet, F., Head, J. W., Mangold, N., Bibring, J. P., Pelkey, S. M., Fassett, C. I., Langevin, Y., and Neukum, G., 2007, Mineralogy of the Nili Fossae region with OMEGA/Mars Express data: 1. Ancient impact melt in the Isidis Basin and implications for the transition from the Noachian to Hesperian: Journal of Geophysical Research-Planets, v. 112, no. E8.

Oluwadebi, A. G., 2011, Characterization of hydrothermal alteration in mount Berecha area of main Ethiopian rift using hyperspectral data: University of Twente Faculty of Geo-Information and Earth Observation (ITC), 62 p.

Poulet, F., 2005, Phyllosilicates on Mars and implications for early martian climate: Nature, v. 438, p. 623-627.

Poulet, F., Bibring, J. P., Mustard, J. F., Gendrin, A., Mangold, N., Langevin, Y., Arvidson, R. E., Gondet, B., and Gomez, C., 2005, Phyllosilicates on Mars and implications for early martian climate: Nature, v. 438, no. 7068, p. 623-627.

Poulet, F., Gomez, C., Bibring, J. P., Langevin, Y., Gondet, B., Pinet, P., Belluci, G., and Mustard, J., 2007, Martian surface mineralogy from Observatoire pour la Minéralogie, l'Eau, les Glaces et l'Activité on board the Mars Express spacecraft (OMEGA/MEx): Global mineral maps: J. Geophys. Res., v. 112, no. E8, p. E08S02.

Poulet, F., Mangold, N., Platevoet, B., Bardintzeff, J. M., Sautter, V., Mustard, J. F., Bibring, J. P., Pinet, P., Langevin, Y., Gondet, B., and Aleon-Toppani, A., 2009, Quantitative compositional analysis of martian mafic regions using the MEx/OMEGA reflectance data 2. Petrological implications: Icarus, v. 201, no. 1, p. 84-101.

Schaber, G. G., 1982, Syrtis major: A low-relief volcanic shield,: J. Geophys.Res., , v. 87, p. 9852–9866.

Smith, D. E., Zuber, M. T., Frey, H. V., Garvin, J. B., Head, J. W., Muhleman, D. O., Pettengill, G. H., Phillips, R. J., Solomon, S. C., Zwally H, J., and Banerdt, W. B. a. D., T. C., 1998, Topography of the northern hemisphere of Mars from the Mars Orbiter Laser Altimeter: Science, v. 279, p. 1686-1692.

Thomas, M., and Walter, M.R., 2002, 'Application of hyperspectral infrared analysis of hydrothermal alteration on Earth and Mars': Astrobiology v. 2, no. 3, p. 335-351.

Zuber, M. T., D.E. Smith, S.C. Solomon, D.O. Muhleman, J.W. Head, J. B. G., and J.B. Abshire, a. J. L. B., 1992, The Mars Observer Laser Altimeter investigation: J. Geophys. Res. , v. 97, p. 7781-7798. .